CHAPTER-5

CHAPTER 5

TRIBOLOGICAL BEHAVIOUR OF TEXTURED DISC IN LUBRICATED CONDITION

This chapter presents the results on the friction and wear behaviour of untextured (UT), and textured steel specimens, i.e., CT7, CT20, BT7 and BT20 slid at different normal loads of 10, 30, and 50 N and sliding speeds of 0.2, 0.8, 1.4, and 2.0 m/s under single drop lubrication. The observed behaviour has been discussed in the light of the worn surface features to unravel the effect of the shape and density of textures on the friction and wear performance of bearing steel.

5.1 EFFECT OF LASER SURFACE TEXTURING ON THE FRICTION AND WEAR PROPERTIES

5.1.1 FRICTION BEHAVIOUR

Figure 5.1 (a) shows the variation of the coefficient of friction for an untextured (UT) surface in single drop lubrication with the number of revolutions at different speeds of 0.2, 0.8, 1.4, and 2.0 m/s under a constant load of 10 N. The variation shows a typical fluctuating tendency at all speeds. At all speeds except 0.2 m/s, the coefficient of friction rises initially and then fluctuates around a steady average value. At 0.2 m/s, the coefficient of friction decreases as the number of revolutions increases.

Figure 5.1 (b) depicts the variation of the coefficient of friction with the number of revolutions at a constant load of 10 N and different speeds of 0.2 m/s, 0.8 m/s, 1.4 m/s, and 2.0 m/s for CT7 in single drop lubrication. One may observe that the coefficient of friction is initially large for all the speeds. However, the value diminishes after ~ 250 revolutions and remains stable thereafter till the full duration of the test with small fluctuations except for 0.2

m/s, which shows a slightly increasing trend with the increasing number of revolutions. It may also be noticed that the amplitude of fluctuation is quite less for the textured specimen, CT7 (Fig. 5.1 (b)), in comparison to the untextured one (Fig. 5.1 (a)).

The variation of coefficient of friction under single drop lubrication for CT20 with the number of revolutions at different speeds and at a constant load of 10 N is presented in Fig. 5.1 (c). A drop in the coefficient of friction could be seen after a certain number of revolutions before attaining a steady value at all speeds, which remains stable till the end of the test. However, the drop is very drastic at the lowest speed of 0.2 m/s, and the value is observed to decrease from 0.49 to 0.1 after sliding 1200 cycles and remains almost constant until the end of the test. At 0.8 m/s and 1.4 m/s, the coefficient of friction begins to decrease after 2000 revolutions and stabilizes thereafter. The coefficient of friction is found to attain a steady value after running for 4000 revolutions at 2.0 m/s. One may also observe that the fluctuation in amplitude is very less.

The variation in coefficient of friction with the number of revolutions under single drop lubrication for BT7 shown in Fig. 5.1 (d) shows that there is a decline in the value of the coefficient of friction after ~ 100 revolutions for all the speeds, which remains stable until the entire duration of the test. However, the coefficient of friction lies between 0.05 and 0.10 for BT7 for all the speeds. One may also observe a relatively large fluctuation in amplitude at the lowest speed of 0.2 m/s in comparison to that observed for speeds of 0.8, 1.4, and 2.0 m/s.

The variation in the coefficient of friction with a number of revolutions for BT20 at different speeds and at a constant load of 10 N shown in Fig. 5.1 (e) also reveals a typical fluctuating trend. At all the speeds, the value falls after a given number of revolutions. After 1000 cycles of sliding, the coefficient of friction for BT20 reduces from 0.38 to 0.10 and remains constant for 0.2 m/s and 0.8 m/s until the end of the test. At higher speeds of 1.4 and

2 m/s, the value becomes stable after 3000 revolutions. It can also be observed that at higher speeds, the amplitude of variation is slightly less than that at 0.2 m/s.

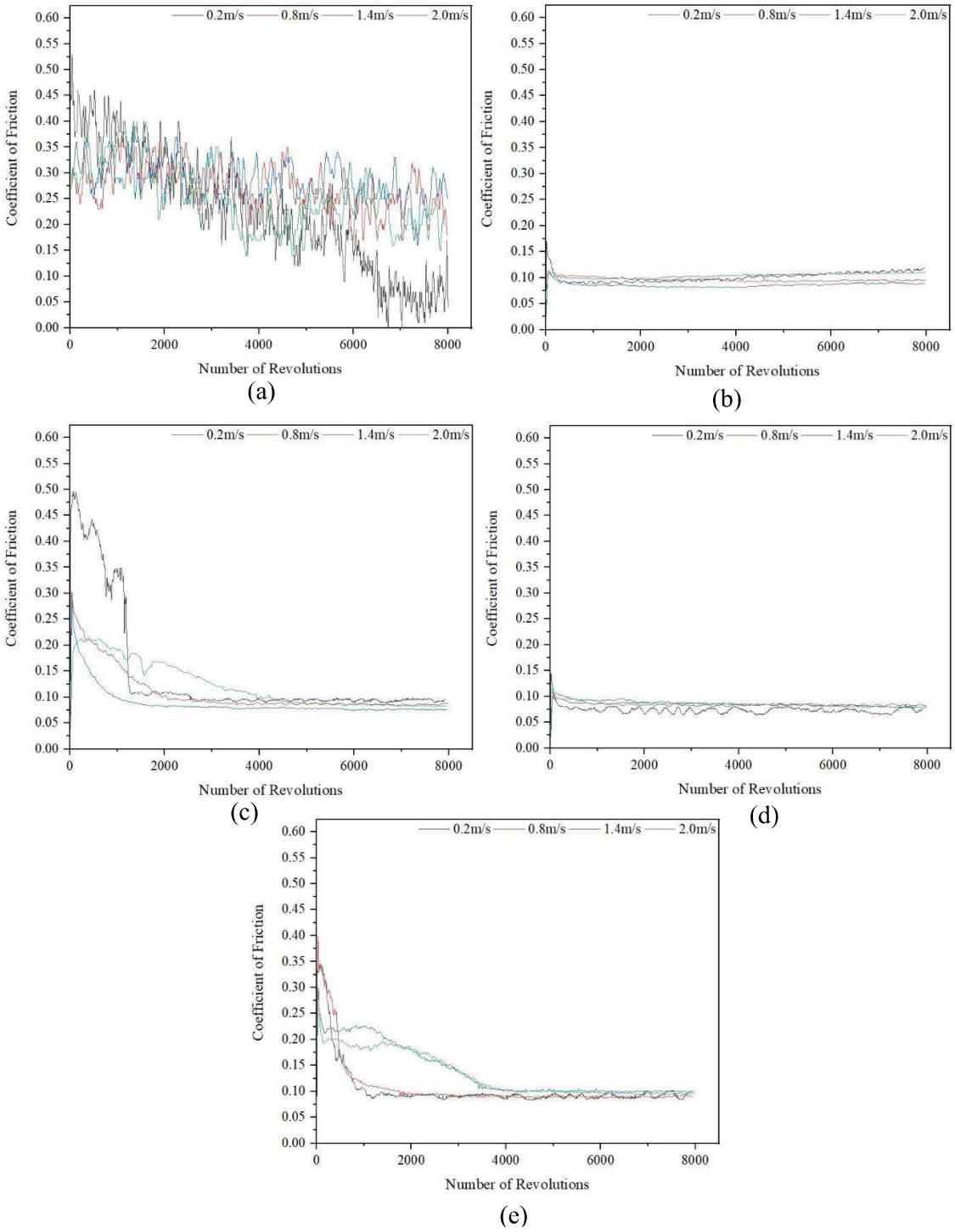

Fig. 5.1 Variation of coefficient of friction with number of revolutions at different speeds and a constant load of 10 N for (a) UT, (b) CT7, (c) CT20, (d) BT7 and, (e) BT20

Figure 5.2 (a) depicts the variation in the coefficient of friction for UT in single drop lubrication with a constant load of 30 N and a number of revolutions at speeds of 0.2, 0.8, 1.4, and 2.0 m/s. For all the speeds, the variation exhibits a fluctuating trend. After a minor gain in value, the coefficient of friction reduces and stays close to 0.22 until 3000 rotations, then drop to 0.2 after a slight rise in value. After a decline from 0.24 to 0.21 at 0.8 m/s, the coefficient of friction fluctuates around 0.21. At roughly 5000 revolutions, the magnitude of the fluctuation increases and then reduces to 0.2 until 8000 revolutions. After falling to 0.19 at 1.4 m/s, the coefficient of friction increases to 0.21 after 1000 rotations before falling to 0.19 again. The value rises to 0.26 after 6000 revolutions and remains fluctuating until the completion of the test. The coefficient of friction declines to 0.21 at 2 m/s, with a minor rise and dip near 1000 revolutions, and remains stable until 8000 revolutions.

Figure 5.2 (b) displays the variation of coefficient of friction with the number of revolutions at a constant load of 30 N and speeds of 0.2, 0.8, 1.4, and 2.0 m/s for CT7 under single drop lubrication. The coefficient of friction drops to 0.09 and shows a relatively larger amplitude of fluctuation at 0.2 m/s till the completion of the test, whereas at 0.8 m/s, the value declines from 0.13 to 0.09 after 250 revolutions and then rises to 0.1 until 1500 rotations, where it remains constant until the test is completed. The coefficient of friction falls from 0.13 to 0.085 at 1.4 m/s and then stays between 0.08 and 0.09 till 6000 revolutions which is followed by an increase to 0.09 as the test progresses. The coefficient of friction decreases at a higher pace at 2 m/s, reaching 0.07 after 2000 cycles, before steadily decreasing to 0.065 for the remaining test duration.

The variation in the coefficient of friction for CT20 with the number of revolutions at different speeds and a constant load of 30 N in single drop lubrication presented in Fig. 5.2 (c) shows a decrease in value from 0.18 to roughly 0.08 after 500 revolutions for all the speeds. However, the coefficient of friction has shown a fluctuating trend of amplitude between 0.08

and 0.11 at the lowest speed of 0.2 m/s, whereas it remains steady with only marginal fluctuations in amplitude at other speeds, i.e., 0.8, 1.4, and 2.0 m/s. The value of the coefficient of friction is observed to be 0.09 at speeds of 0.8 and 2 m/s, while at 1.4 m/s, it is found to be 0.10.

The variation in coefficient of friction for BT7 with the number of revolutions at different speeds and a constant load of 30 N is shown in Fig. 5.2 (d). After around 500 rotations at 0.2 m/s, the coefficient of friction drops from 0.16 to 0.0.09, and there is significant fluctuation in the amplitude for the full duration of the test. However, at higher speeds, the coefficient of friction remains almost stable with only slight fluctuations in amplitude. The coefficient of friction is observed to be the lowest at 2 m/s.

Figure 5.2 (e) shows the variation of coefficient of friction with the number of revolutions in single drop lubrication for BT20 at different speeds and a constant load of 30 N. After approximately 500 cycles at all speeds, the value falls from 0.22 to 0.09. The coefficient of friction is found to fluctuate significantly for 8000 revolutions at the lowest speed of 0.2 m/s. However, the variation in coefficient of friction is observed to be stable at higher speeds for the complete duration of the test, and values appear to fall in a narrow band for all these speeds, i.e., 0.8, 1.4, and 2.0 m/s.

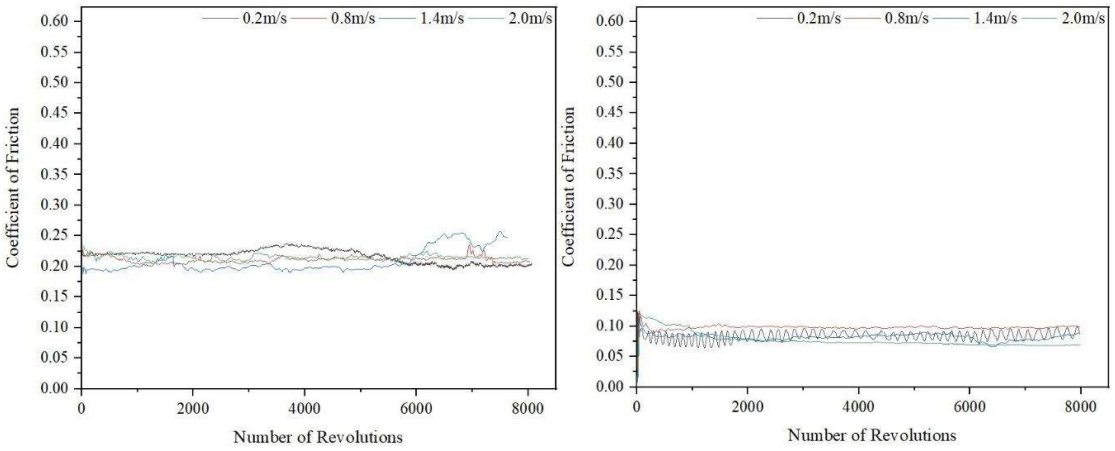

(a) (b)

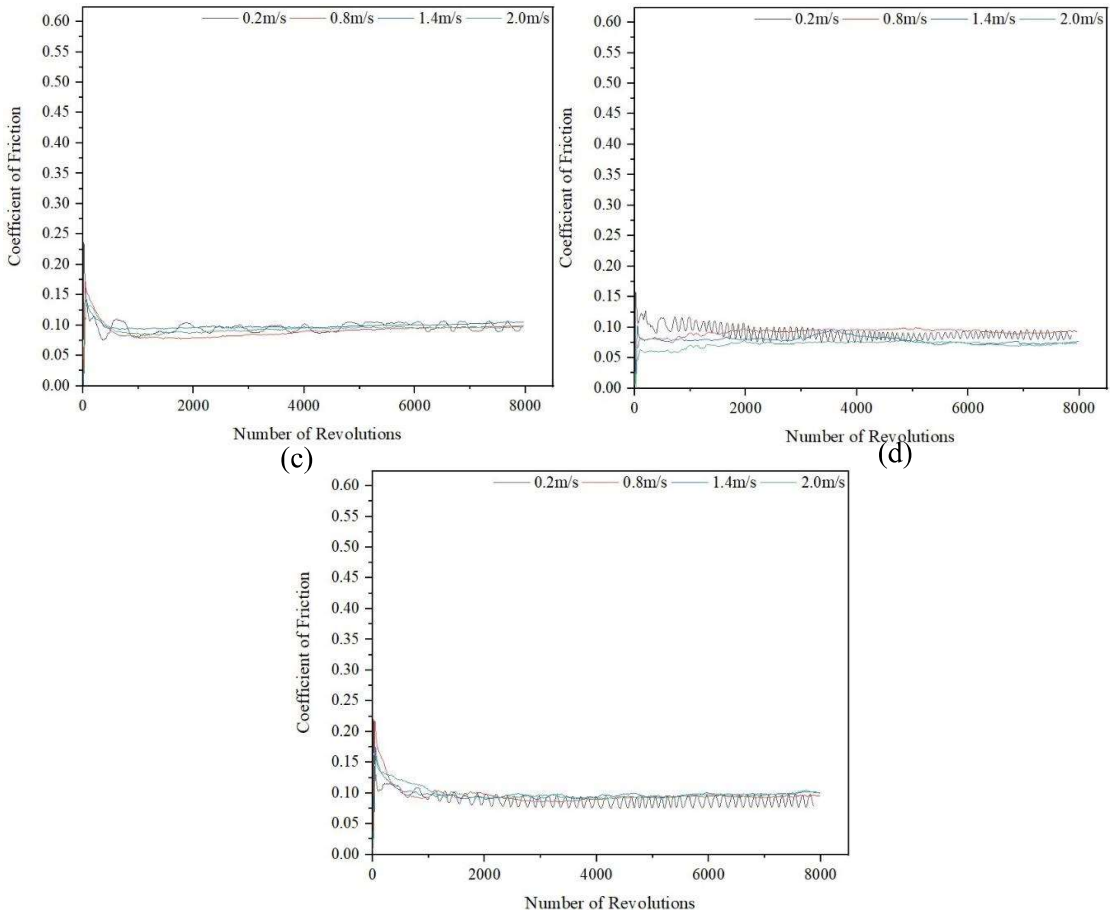

Fig. 5.2 Variation of coefficient of friction with the number of revolutions at different speeds and a constant load of 30 N for (a) UT, (b) CT7, (c) CT20, (d) BT7, and, (e) BT20

Figure 5.3 (a) shows the variation of coefficient of friction for UT with the number of revolutions at different speeds and a constant load of 50 N in single drop lubrication. The coefficient of friction at 0.2 m/s declines from 0.23 to about 0.20 after 500 cycles and remains steady until the test is completed. After a reduction from 0.21 to around 0.19, the coefficient of friction indicates a modest gain at 0.8 m/s, which it maintains until 3000 revolutions. For the rest of the revolutions, a progressively increasing trend with a maximum coefficient of friction of 0.21 can be noted. After a modest decline at 1.4 m/s, the coefficient of friction rises from 0.12 to 0.18 and remains steady for 7000 cycles. After that, the value gradually rises to 0.19 until the end of the test. At the highest speed of 2 m/s, the coefficient of friction drops to

0.17 after 250 cycles and then gradually falls to 0.16 during the next 2500 revolutions before rising to 0.23 for the remaining duration of the test.

The variation of coefficient of friction for CT7 with the number of revolutions at different speeds and a constant load of 50 N in single drop lubrication is shown in Fig. 5.3 (b). At all speeds, there is a usual decrease in the coefficient of friction after a certain number of revolutions. At 0.2 m/s, and 1.4 m/s there is a considerable fluctuation in amplitude, which has decreased at 0.8 m/s, and 2 m/s. The coefficient of friction lowers from 0.35 to around 0.18 at 0.2 m/s and stays there until the completion of the test. As the test progresses, the magnitude of variation gradually decreases. Beyond 1000 revolutions, the coefficient of friction declines from 0.3 to around 0.16 at 0.8 m/s, and a further drop to 0.13 can be seen until 3000 revolutions. For the rest of the revolutions, there is a progressive increase in the value to 0.15. The coefficient of friction declines from 0.23 to 0.10 at 1.4 m/s until 2000 revolutions, then continue with some fluctuations until 6000 revolutions. One may observe that after a rapid decrease and rise at roughly 6800 revolutions, the value increases again for the rest of the revolutions, with a maximum coefficient of friction of about 0.20 at the end of the test. The coefficient of friction lowers from 0.25 to 0.10 after 2000 cycles at the highest speed of 2 m/s. The value is maintained with a slight increase to about 0.12 for the rest of the revolutions.

Figure 5.3 (c) shows the variation of the coefficient of friction for CT20 with the number of revolutions at different speeds and a constant load of 50 N in single drop lubrication. The variation has a lot of fluctuation at the lowest speed of 0.2 m/s, but it's nearly non-existent at higher speeds. For about 500 cycles, a decrease in the coefficient of friction can be seen at all speeds. At 0.2 m/s, the value drops from 0.12 to 0.08 and occurs for 4000 cycles which continues for the rest of the revolutions with a slight increase. After a typical decline near 500 cycles, the coefficient of friction rises to 0.13 at 0.8 m/s until 2000 cycles. For the rest of the rotations, the coefficient of friction gradually decreases until it reaches a minimum value of

0.12. After the usual drop, the coefficient of friction remains around 0.13 at 1.4 m/s for the rest of the revolutions. At 2 m/s, the coefficient of friction drops from 0.12 to 0.08 and continues with a gradual decline to about 0.065 until 7000 revolutions before rising marginally till the completion of the test.

The variation in coefficient of friction for BT7 with the number of revolutions at different speeds and a constant load of 50 N is shown in Fig. 5.3. (d). The coefficient of friction increases for 2000 cycles at 0.2 m/s and then declines for the rest of the rotations with a significant fluctuation in its amplitude. The first dip to 0.10 is barely noticeable, and the tendency eventually equalizes at the end of the test. The coefficient of friction climbs from 0.02 for roughly 4000 cycles at 0.8 m/s following the typical decline, with exceptional amplitude variation. Following that, the coefficient of friction drops for the next 500 revolutions, and then rises with the fluctuation near the end of the test, with a final drop in the value. The coefficient of friction is lower at higher speeds of 1.4 and 2 m/s and remains constant until the completion of the test. The coefficient of friction, on the other hand, is lowest at 2 m/s and displays a drop and climb in value at 3000 revolutions.

The variation of the coefficient of friction for BT20 with the number of revolutions at different speeds and a constant load of 50 N in single drop lubrication is shown in Figure 5.3 (e). At a low speed of 0.2 m/s, the coefficient of friction shows significant fluctuation in amplitude until the end of the test. The coefficient of friction remains constant at roughly 0.11 at 0.8 m/s until the completion of the test. The variation in coefficient of friction at 1.4 m/s shows a rise in the value near 3000 revolutions and continues at this value until the end of the test. The variation has fluctuation for all the revolutions. The coefficient of friction at 2 m/s remains constant until 4000 cycles, then increase with fluctuation for the rest of the rotations, culminating in a final plunge.

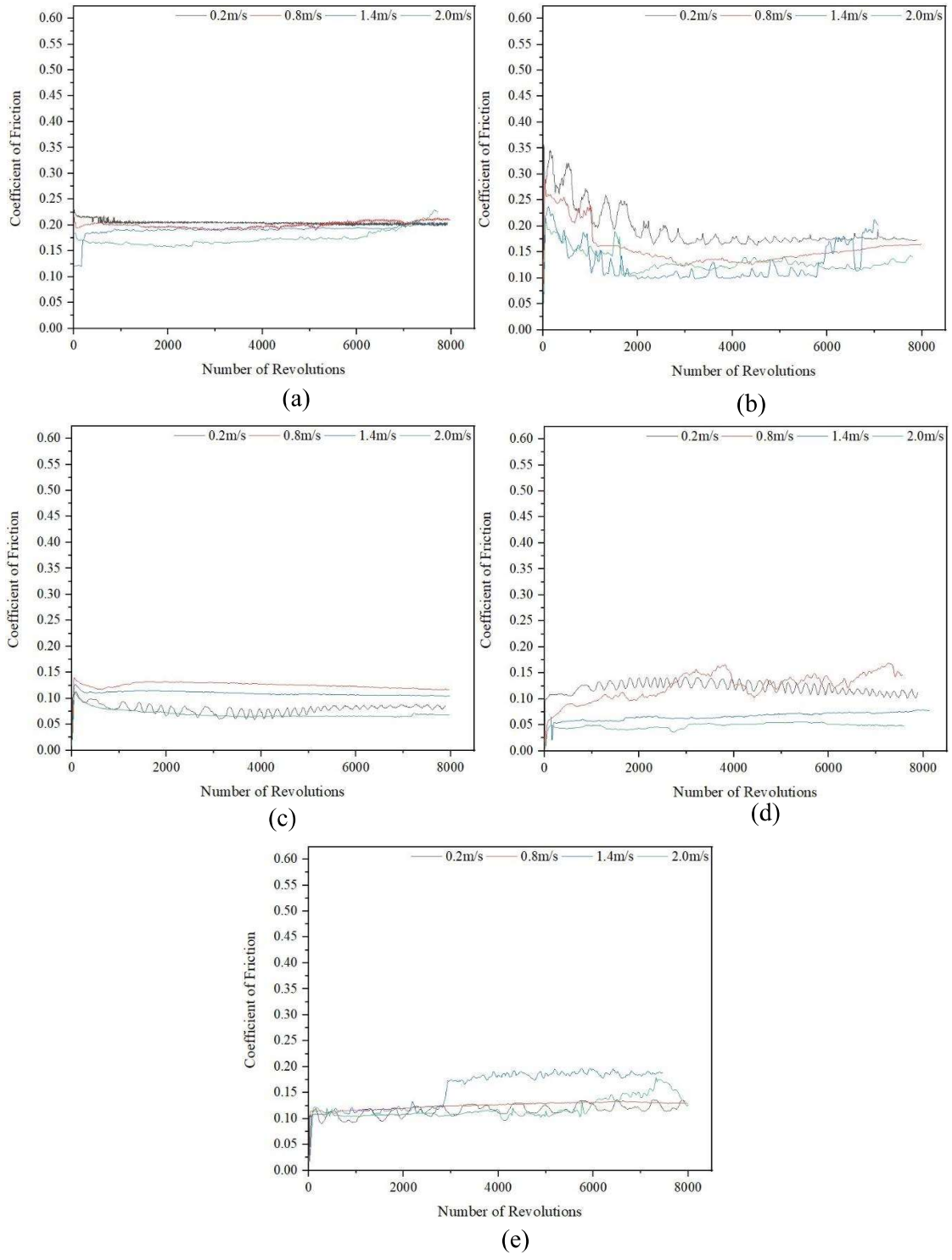

Fig. 5.3 Variation of coefficient of friction with number of revolutions at different speeds and a constant load of 50 N for (a) UT, (b) CT7, (c) CT20, (d) BT7 and, (e) BT20

Figure 5.4 shows the variation of the average coefficient of friction with speed for UT, CT7, CT20, BT7, and BT20 at a constant load of 10N. The coefficient of friction for UT is observed to increase with increasing speed from 0.2 to 1.4 m/s, followed by a decrease thereafter and the value varies from 0.22 to 0.28. One may observe an increase in the average coefficient of friction as the speed is increased from 0.2 m/s to 2.0 m/s for samples having Bi-triangular dimples i.e., BT7 and BT20. However, the increase in the average coefficient of friction is relatively less for BT7 than that for BT20. In contrast, the average coefficient of friction is found to decrease sharply for specimens having circular dimples i.e., CT7 & CT20, as the speed is raised from 0.2 m/s to 1.4 m/s and increases as the speed is increased to 2.0 m/s. The average coefficient of friction at any speed is also found to be relatively lower for a lesser fraction of area coverage by the dimples, i.e., for BT7 and CT7, and higher for an increased fraction of area coverage (BT20 and CT20) which highlights the effect of dimple density on the frictional performance. At a particular speed (say 0.2 m/s), the average coefficient of friction observed for the sample having 7% density with bi-triangular shape (BT7) is the lowest and that for the sample having 20% density with circular dimples (CT20) is the highest. The value of the coefficient of friction for CT7 and BT20 falls in-between, with CT7 having a lower coefficient of friction than BT20, reflecting thus, the combined effect of density and shape of the dimples on friction reduction. A similar pattern of variation is also observed at the other speeds, as evident from Fig. 5.4. However, BT7 has shown the lowest coefficient of friction at all the speeds indicating that it is the optimum dimple density and shape under the conditions used in the current investigation.

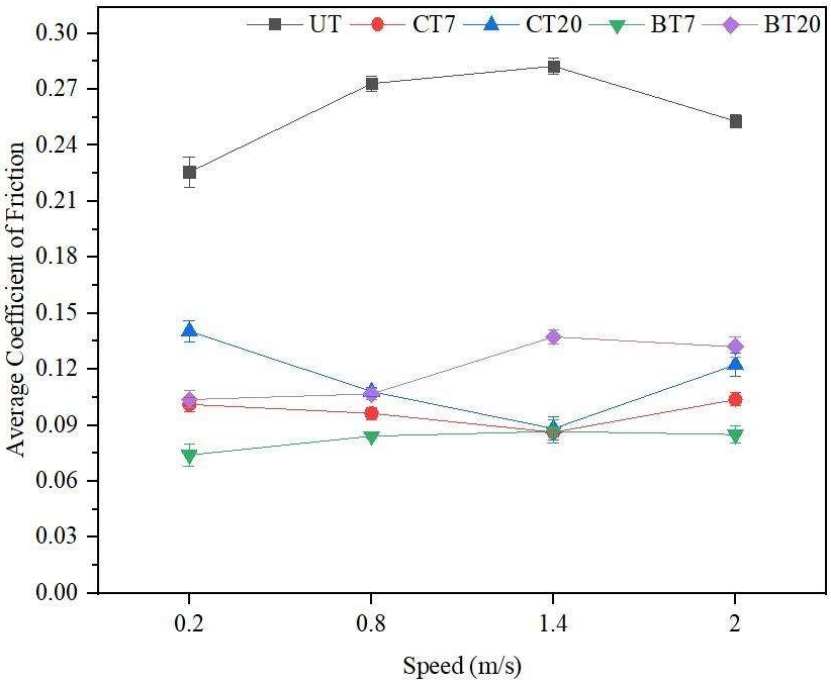

Fig. 5.4 Average coefficient of friction for various samples at different speeds and at a constant load of 10 N

The variation of the average coefficient of friction with speed for UT, BT7, CT7, BT20, and CT20 under single drop lubrication at a constant load of 30N is illustrated in Fig. 5.5. The textured samples have a lower average coefficient of friction in comparison to Untextured. The coefficient of friction for UT is observed to decrease with increasing speed from 0.2 to 1.4 m/s, followed by an increase thereafter, and the value varies from 0.21 to 0.22. One may observe an increase in the average coefficient of friction as the speed is increased from 0.2 m/s to 0.8 m/s, and at 1.4 m/s the value again decreases before increasing to 2 m/s for BT20. The coefficient of friction for CT7 increases from 0.2 m/s to 0.8 m/s; however, a decrease in the value for CT20 can be observed for this speed range. The average coefficient of friction for CT7 falls as speed increases from 0.8 to 2 m/s, whereas it remains almost equivalent for CT20 in this speed range. In contrast, an increase in the average coefficient of friction for both BT20 and CT20 can be seen with increasing speed from 0.8 m/s to 2 m/s.

Beyond 0.8 m/s, the average coefficient of friction decreases for the lower density of dimples which has the lowest value for BT7 and increases with increasing density of dimples. The specimen with 20% bi-triangular dimples i.e., BT20 has the lowest coefficient of friction at 0.2 m/s and 1.4 m/s when slid at a load of 30 N. Both BT7 and BT20 show a similar trend for all the speeds with close values of the average coefficient of friction.

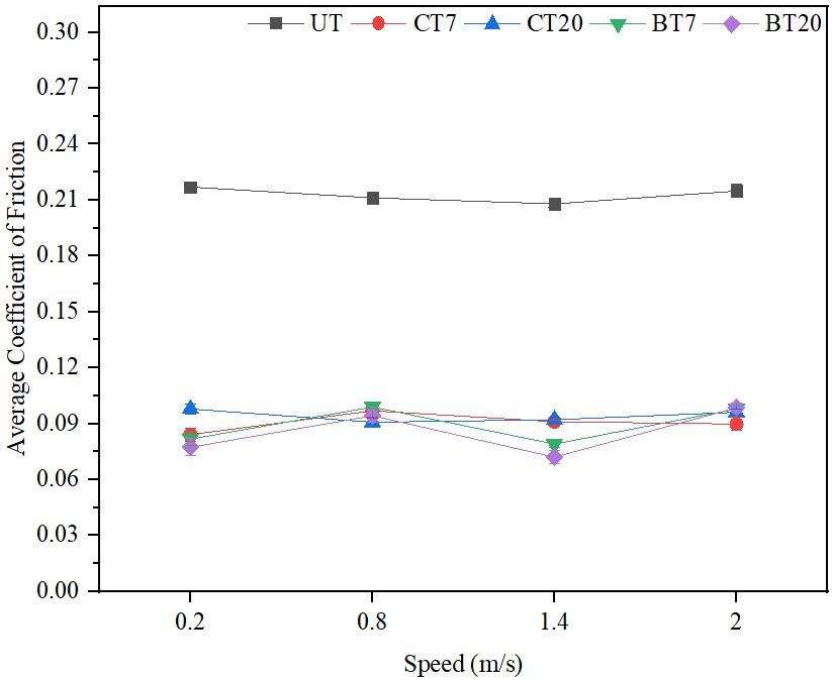

Fig. 5.5 Average coefficient of friction for various samples at different speeds and at a constant load of 30 N

Figure 5.6 shows the variation of the average coefficient of friction with speed for the UT, BT7, CT7, BT20, and CT20 under single drop lubrication at a constant load of 50 N. The textured samples have been observed to show a relatively lower average coefficient of friction than the untextured samples. The average coefficient of friction for the untextured sample as well as CT7 is found to decrease with an increase in speed from 0.2 to 2 m/s. One may also observe that the average coefficient of friction for BT20 increases with increasing speed from 0.2 to 1.4 m/s, followed by a marginal decrease till 2.0 m/s. However, the increase in the value

corresponding to an increase in speed from 0.8 to 1.4 m/s is a bit sharp in comparison to the one corresponding to the increase between 0.2 to 0.8 m/s. The average coefficient of friction for CT20 and BT7 has been found to decrease continuously with increasing speed. The decrease is marginal in the range of speed from 0.2 m/s to 0.8 m/s. However, the coefficient of friction is found to drop significantly beyond 0.8 m/s for both CT20 and BT7, with BT7 showing a relatively larger drop. The average coefficient of friction by BT7 is consistently lower than other specimens at all speeds except at 0.2 m/s, where BT20 has a slightly lower coefficient of friction.

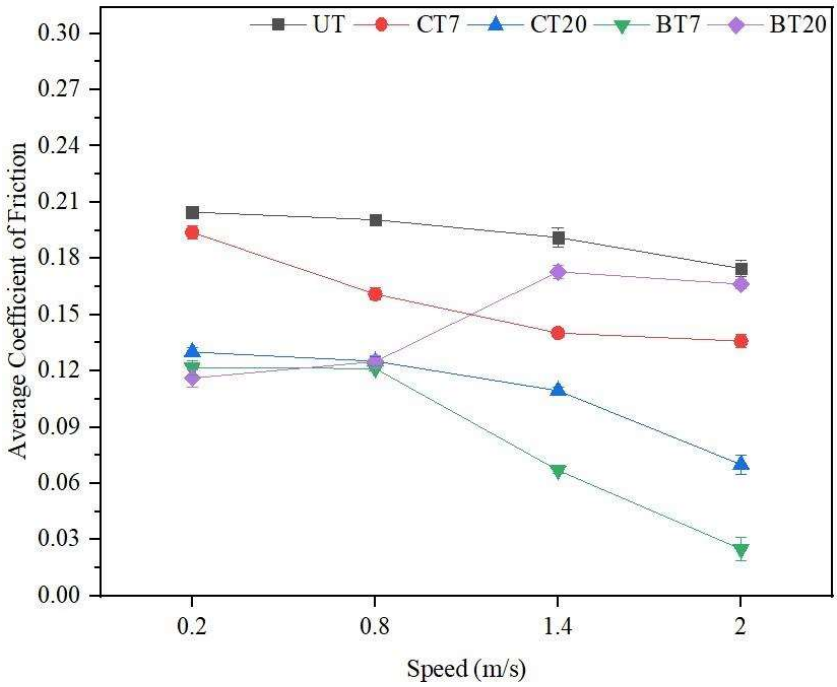

Fig. 5.6 Average coefficient of friction for various samples at different speeds and at a constant load of 50 N

Figure 5.7 illustrates the variation in the average coefficient of friction with load at a fixed sliding speed of 0.2 m/s for UT as well as textured steel. UT shows a decrease in the value from 0.225 to 0.204 as the load is increased from 10 to 50 N. However, UT has shown the highest coefficient of friction among all the specimens. CT7, CT20, and BT20 exhibit the

same trend of variation i.e., the average friction coefficient first decreases as the load is raised from 10 to 30 N which is followed by a rise in the average coefficient of friction till 50 N. However, BT7 shows a gradual rise in the average coefficient of friction from 0.074 to 0.122 as the load increased from 10 to 50 N.

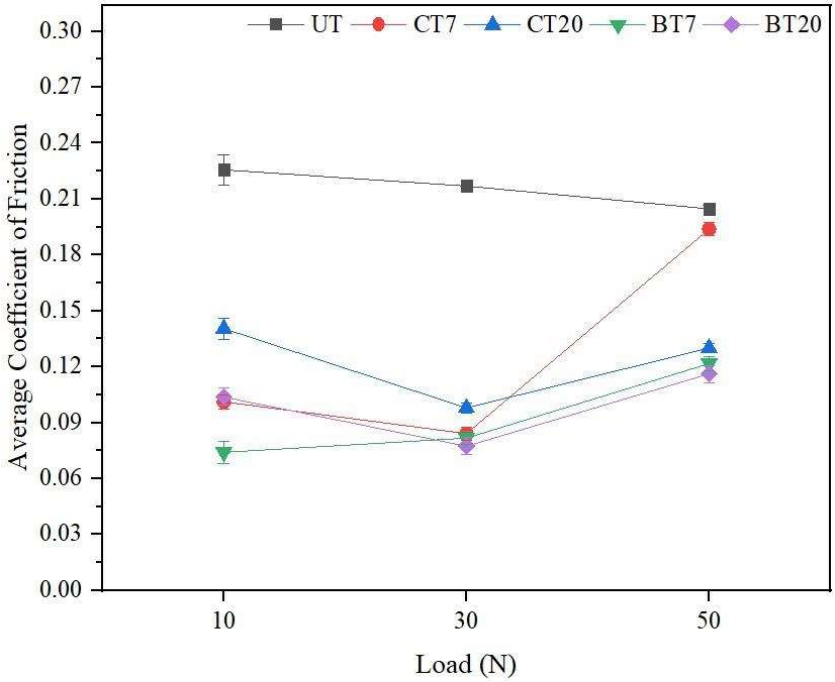

Fig. 5.7 Average coefficient of friction for various samples at different loads and at a speed of 0.2 m/s

The variation in the average coefficient of friction with load at a fixed sliding speed of 0.8 m/s is presented in Fig. 5.8 for all the specimens used in the present study. One may again observe a continuous decrease in the coefficient of friction as the load is increased from 10 to 50 N. For CT7, the average coefficient of friction is observed to remain the same with an increase in load from 10 to 30 N which is followed by a significant rise in value for 50 N. CT20 and BT20 show a slight decrease in the average coefficient of friction value as the load increases from 10 to 30 N, and a rise to around 0.125 is observed thereafter for a 50 N load. However, BT7exhibits a gradual rise in the value from 0.084 to 0.121as the load increases from

10 N to 50 N. BT7 indicates the lowest value observed at 10 N load. It may also be observed that the values of average coefficient of friction for CT7, CT20, BT7, and BT20 fall in a close band at loads of 30 and 50 N barring an exception of CT 20, which shows significantly higher values at 50 N as evident from Fig. 5.8. However, at the lowest load of 10 N there appears to be a slight difference in the values with BT7 showing the lowest value.

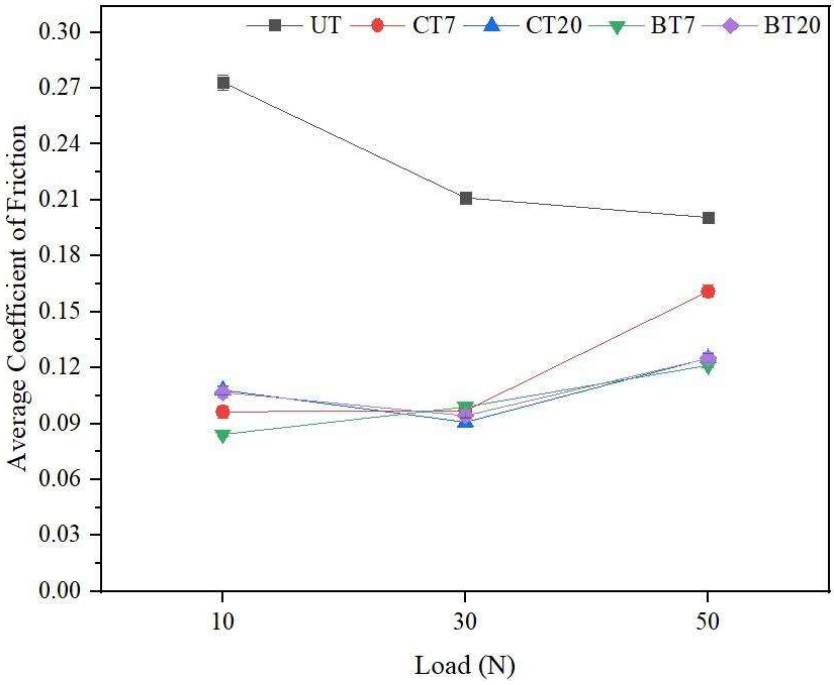

Fig. 5.8 Average coefficient of friction for various samples at different loads and at a speed of 0.8 m/s

Figure 5.9 shows the variation in the average coefficient of friction at different loads for a 1.4 m/s speed. UT shows a decrease in the average coefficient of friction value from 0.282 to 0.191 as the load is increased from 10 N to 50 N. With an increasing load from 10 N to 50 N, CT7 exhibits a rise in the average coefficient of friction from 0.086 to 0.140. An increase in the average coefficient of friction value from 0.088 to 0.109 can be observed in the case of CT20 as the load increases from 10 N to 50 N. BT7 exhibits a decrease in the value from 0.086 at 10 N to 0.067 at 50 N load, whereas BT20 indicates a decrease in the average coefficient of

friction to about 0.137 at 10 N and 0.072 at 30 N loads which increases to 0.173 with the increase in load to 50 N. BT7 has the lowest average coefficient of friction at 50 N when compared to the other specimens.

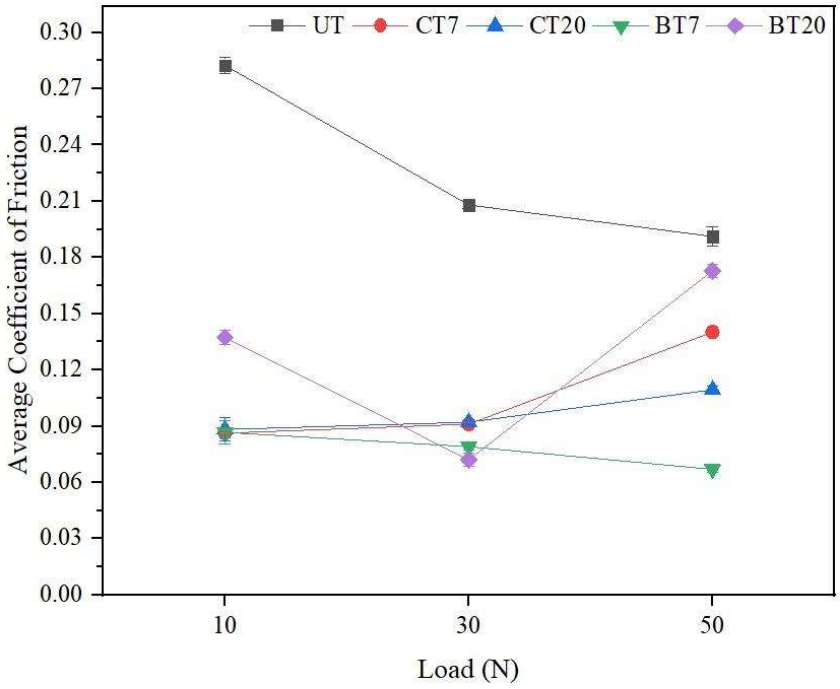

Fig. 5.9 Average coefficient of friction for various samples at different loads and at a speed of 1.4 m/s

Figure 5.10 depicts the variation in the average coefficient of friction under various loads at a speed of 2.0 m/s. As the load is raised from 10 N to 50 N, UT displays a drop in the average coefficient of friction value from 0.253 to 0.175. The average coefficient of friction of CT7 and BT20 increases as the load increases from 10 N to 50 N, with a slight decrease at 50 N. When the load is increased from 10 N to 30 N, the average coefficient of friction for BT7 increases, but when the load is increased to 50 N, the average coefficient of friction decreases. CT20 shows a drop in the value from 0.122 to 0.070 with increasing load. At 10 N and 50 N, BT7 has the lowest average coefficient of friction of all the specimens.

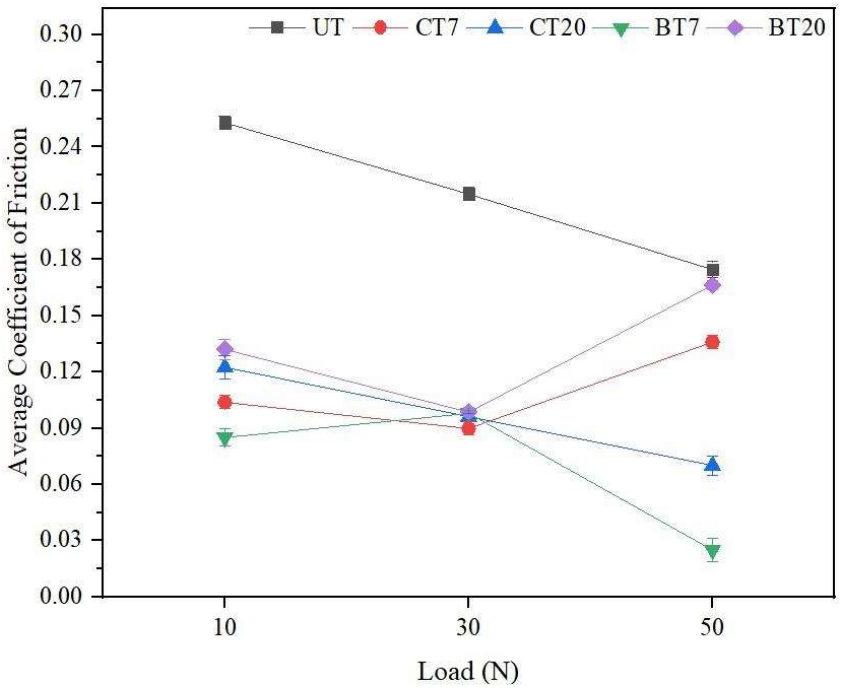

Fig. 5.10 Average coefficient of friction for various samples at different loads and at a speed of 2 m/s

5.1.2 WEAR BEHAVIOUR

Figure 5.11 shows the variation of wear rate for UT, CT7, CT20, BT7, and BT20 at various sliding speeds of 0.2, 0.8, 1.4, and 2.0 m/s under a constant load of 10 N. The wear rate of UT is observed to decrease with an increase in speed. At the speeds of 0.8 m/s and 1.4 m/s, the variation in wear rate is less as compared with the variation at 0.2 m/s and 2.0 m/s. The wear rate for BT7 & CT7 has been observed to decrease with increasing speed from 0.2 m/s to 2.0 m/s, whereas for CT20, it is observed to decrease sharply as the speed is raised from 0.2 m/s to 1.4 m/s before increasing for a speed of 2.0 m/s as seen from Fig. 5.11. However, the wear rate for BT20 is found to decrease as the speed is increased from 0.2 m/s to 0.8 m/s before increasing again at a speed of 1.4 m/s, followed by a decrease at 2.0 m/s. One may also observe from Fig. 5.11 that the wear rate is less for the specimens having a relatively lower density of dimples for both bi-triangular and circular shapes at all speeds, which again shows the effect

of density and shape of dimples. The wear rate shown by BT7 is the lowest at all the speeds except at 1.4 m/s, where it appears to be slightly higher than CT7, indicating again that 7% density with a bi-triangular shape is optimum.

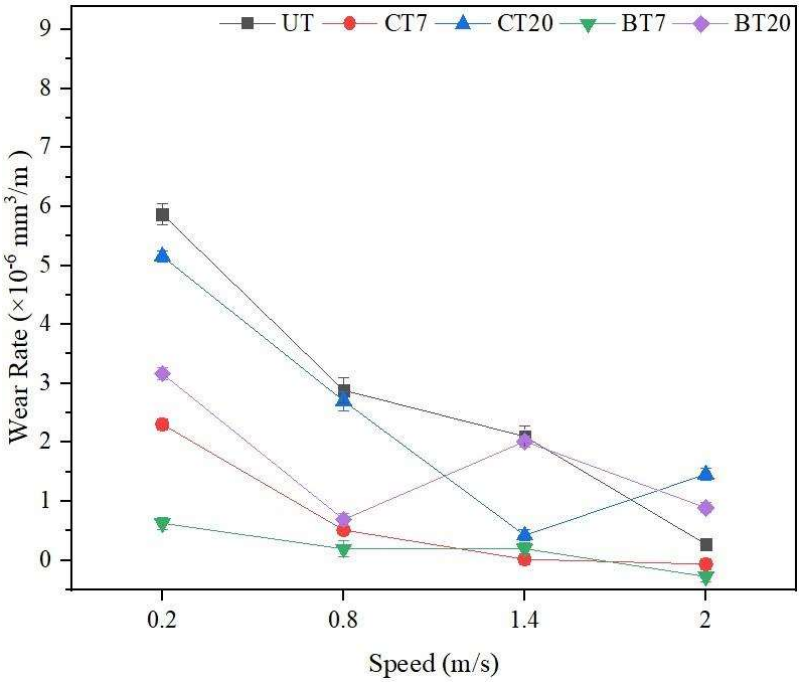

Fig. 5.11 Variation of wear rate in textured specimens at different speeds under a load of 10 N

The variation of wear rate for UT, CT7, CT20, BT7, and BT20 at different sliding speeds of 0.2, 0.8, 1.4, and 2.0 m/s and under a constant load of 30 N is presented in Fig. 5.12. The wear rate of UT steel is observed to decrease with an increase in speed. However, the decrease is relatively sharp as the speed is increased from 0.2 to 0.8 m/s and 1.4 to 2.0 m/s. The wear rate for CT20 has been observed to decrease continuously with increasing speed from 0.2 to 2.0 m/s, whereas for CT7 it decreases from 0.2 to 1.4 m/s and remains almost the same with a further increase in speed to 2.0 m/s. The wear rate of BT20 is observed to be the same at 0.2 and 0.8 m/s and decreases sharply as the speed is increased from 0.8 to 1.4 m/s, beyond which it remains the same till 2.0 m/s. The wear rate of BT7 is found to decrease as the speed is increased from 0.2 to 0.8 m/s, which is followed by a marginal increase with increasing speed

till 2.0 m/s. However, the wear rate shown by BT7 is the lowest at all the speeds at the load of 30 N.

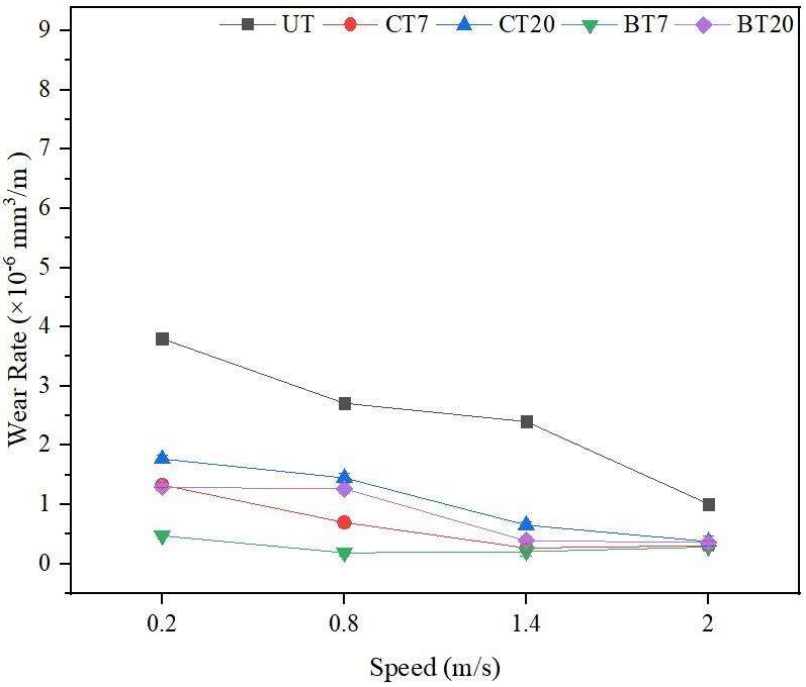

Fig. 5.12 Variation of wear rate in textured specimens at different speeds under a constant load of 30 N

Figure 5.13 shows the variation of wear rate for UT, CT7, CT20, BT7, and BT20 under a constant load of 50 N and different speeds of 0.2, 0.8, 1.4, and 2.0 m/s. The wear rate of UT steel is found to decrease with increasing speed, and it has shown the highest wear rate at all the speeds. The wear rate for CT7 is also observed to decrease with increasing speed, however, the decline is more pronounced between 0.8 and 1.4 m/s. The wear rate of CT20 is seen to decrease with increasing speed from 0.2 to 1.4 m/s followed by an increase as the speed is raised to 2 m/s. However, the decrease in wear rate is quite sharp, between 0.2 to 0.8 m/s. The wear rate for BT7 and BT20 is observed to decrease from 0.2 and 0.8 m/s, followed by an increase till 2.0 m/s. However, the increase is relatively more for BT20 as compared to CT7. It is to be noticed that the wear rates shown for BT7 and CT20 are almost the same at the speeds

of 1.4 and 2.0 m/s when slid under a load of 50 N. It may also be seen that the wear rate shown by BT7 is the lowest at all the speeds after sliding under a constant load of 50 N.

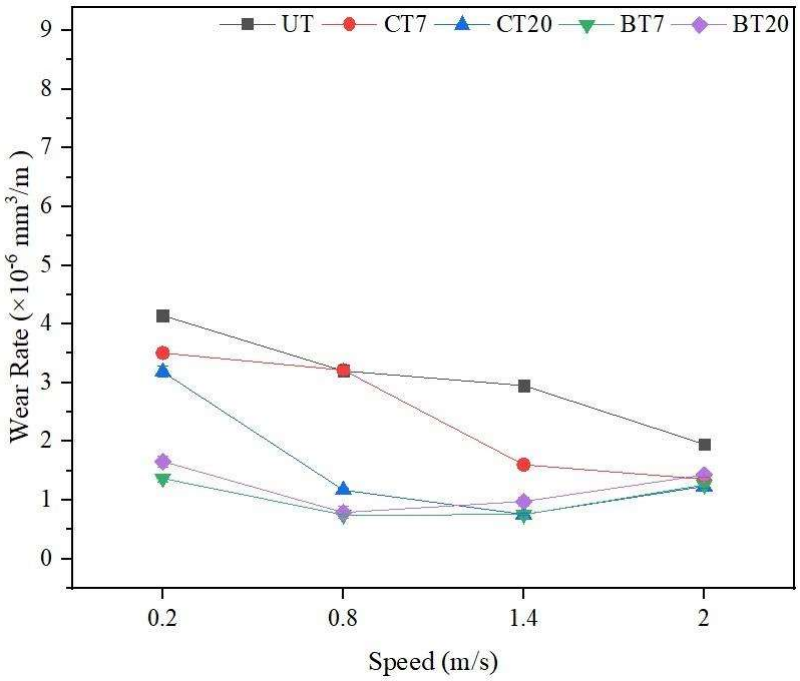

Fig. 5.13 Variation of wear rate in textured specimens at different speeds under a constant load of 50 N

Figure 5.14 shows the variation of wear rate for UT, CT7, CT20, BT7, and BT20 under different loads at a constant speed of 0.2 m/s. One may observe a similar pattern of variation of wear rate with load, i.e., the wear rate if found to decrease from 10 to 30 N followed by an increase thereafter for 50 N for all the specimens. However, the rate of decrease from 10 to 30 N is relatively sharp for CT20 and BT20 in comparison to UT and CT7. As far as an increase in wear rate from 30 to 50 N is concerned, the increase is relatively sharp for CT7 and CT20, whereas it appears to be the same for UT and BT20. One may also observe that the decrease in wear rate from 10 to 30 N is marginal in the case of BT7. However, the wear rate is found to increase from 30 to 50 N, at a rate higher than that observed for UT and BT20. For all loads, the UT specimen has shown the highest wear rate and BT7 the lowest. At loads of 10 and 30 N, CT20 and BT20 have a higher wear rate than CT7 and BT7. The specimen with 7 %

circular dimples, i.e., CT7 has the highest wear rate among all the textured samples at the highest load of 50 N used in the present study.

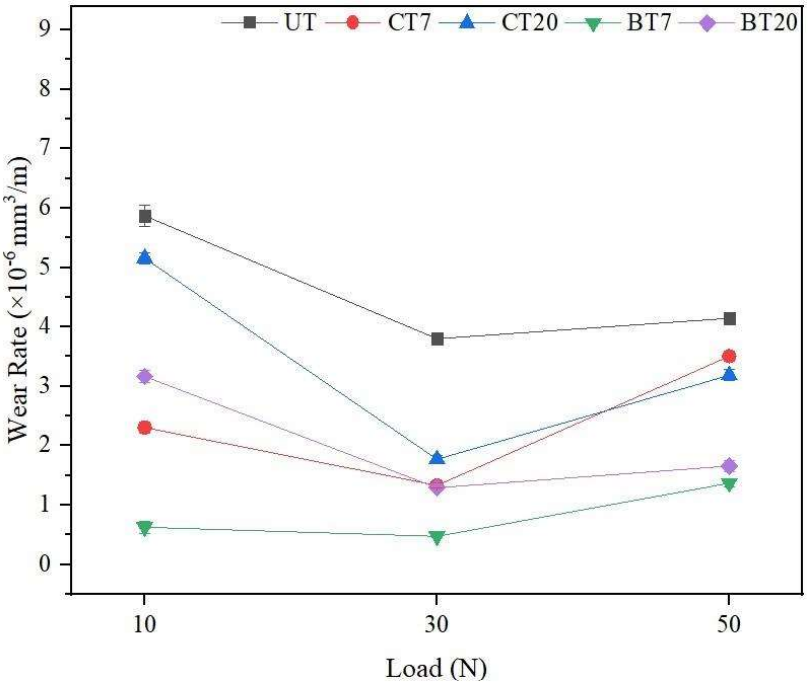

Fig. 5.14 Variation of wear rate in specimens at different loads at a constant speed of 0.2 m/s

Figure 5.15 depicts the variation of wear rate for UT, CT7, CT20, BT7, and BT20 under various loads and at a constant speed of 0.8 m/s. The wear rate for untextured specimen i.e. is observed to decrease from 10 to 30 N followed by an increase for 50 N, and it has shown the highest wear rate at all the loads. The wear rate for CT7 is found to increase as the load is increased from 10 to 50 N with a sharp rise from 30 to 50 N, whereas CT20 has shown a continuously decreasing trend with an increasing load from 10 to 50 N. The wear rate for BT7 is almost found to be the same as 10 and 30 N, whereas it is observed to decrease beyond 30 N. The wear rate for BT20 increases as the load is raised from 10 to 30 N, which is followed by a decrease for 50 N. It may also be noted that BT7 has the lowest wear at all the loads at a speed of 0.8 m/s.

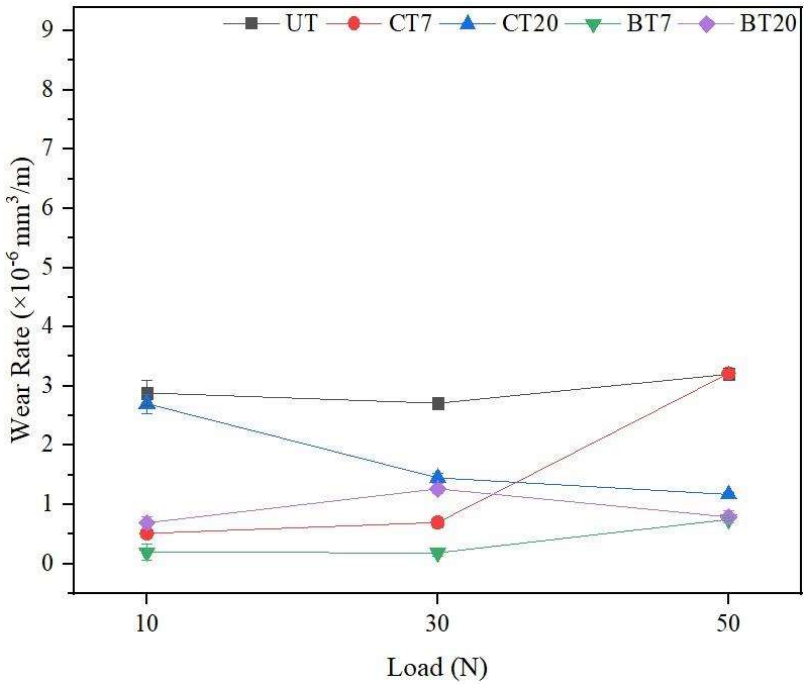

Fig. 5.15 Variation of wear rate in specimens at different loads at a constant speed of 0.8 m/s

The wear rate variation for the UT, CT7, CT20, BT7, and BT20 under varying loads at a constant speed of 1.4 m/s is shown in Fig. 5.16. The wear rate for UT, CT7, CT20, and BT7 has been observed to increase with increasing load from 10 to 50 N, whereas for BT20, it decreases as the load is raised from 10 to 30 N, followed by an increase to 50 N. It may again be noticed that UT has the highest wear rate at all the loads whereas Bt7 has the lowest except at 10 N load, for which CT7 has shown the lowest wear rate.

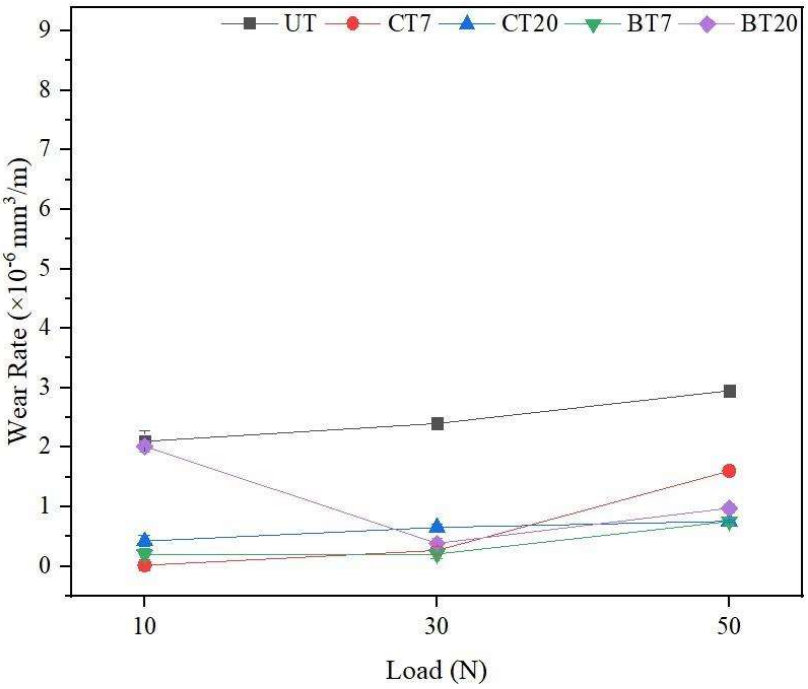

Fig. 5.16 Variation of wear rate in specimens at different loads at a constant speed of 1.4 m/s

Figure 5.17 illustrates the variation of wear rate with load for the UT, CT7, CT20, BT7, and BT20 at a constant speed of 2.0 m/s. The wear rate for UT, CT7, and BT7 has been observed to increase with increasing load from 10 to 50 N, whereas for CT20 and BT20, it decreases from 10 to 30 N, followed by an increase thereafter for 50 N. It may also be noted that CT20 and BT20 have shown relatively higher wear rate at the lowest load of 10 N, whereas at loads of 30 and 50 N UT has the highest wear rate. The wear rate shown by BT7 is the lowest at all the loads, as seen from Fig. 5.17.

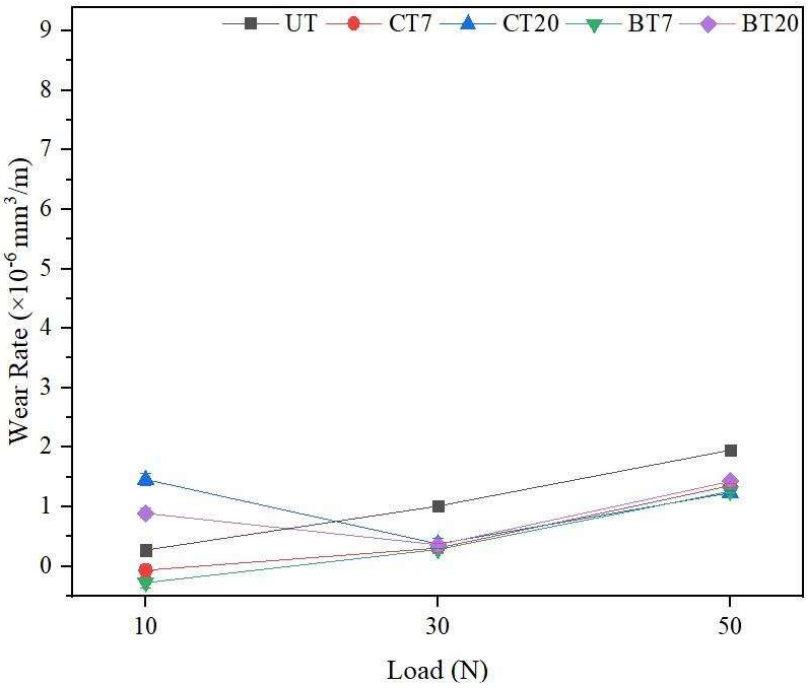

Fig. 5.17 Variation of wear rate in specimens at different loads at a constant speed of 2.0 m/s

5.1.3 WORN SURFACE MORPHOLOGY

The worn surface morphology provides important information regarding the prevailing mechanisms of wear during sliding contact. The worn surface of UT steel is shown in Figs. 5.18 (a-d) at different speeds, which reveals the presence of grooves at all speeds. However, at 0.2 m/s, the grooves are relatively fine and shallow, and the width of the grooves increases with increasing speed until 1.4 m/s before decreasing again at 2.0 m/s, as seen from a comparison of Figs. 5.18 (a, b, c, and d). The grooves are very fine and not much visible as shown in Fig. 5.18 (d). This may explain the increase in the coefficient of friction of UT steel with increasing speed from 0.2 m/s to 1.4 m/s, followed by a decrease at 2.0 m/s, as seen from Fig. 5.4.

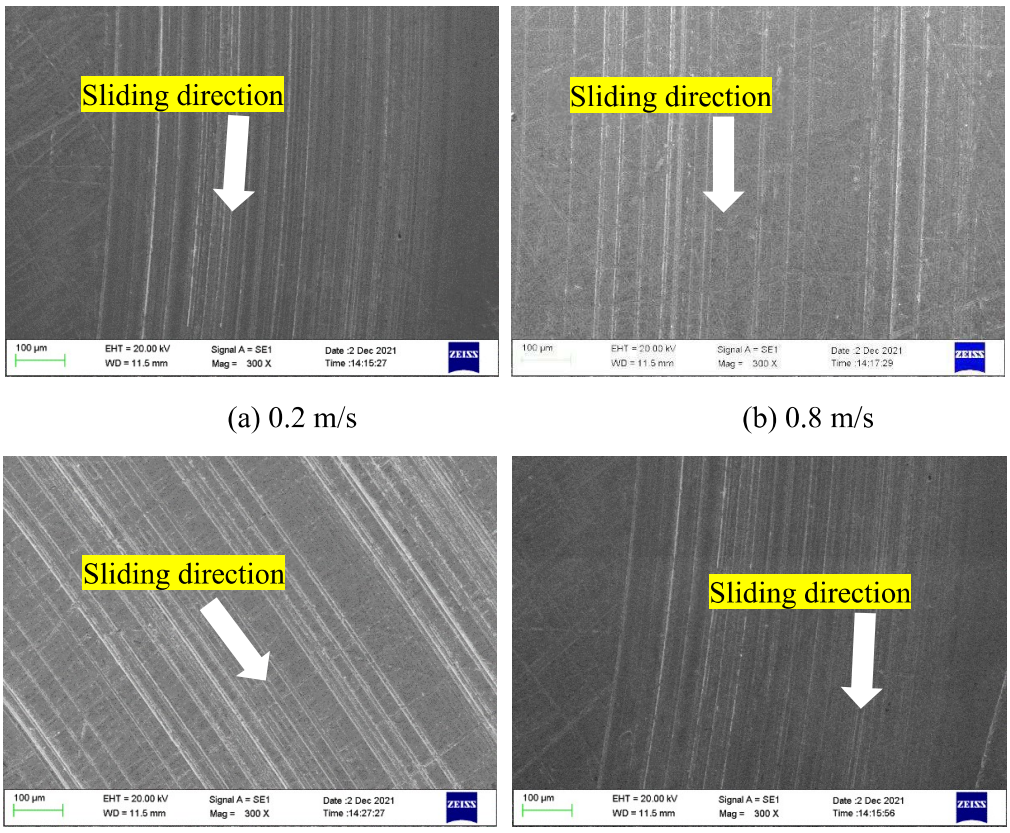

(a) 0.2 m/s (b) 0.8 m/s

(c) 1.4 m/s (d) 2.0 m/s

Fig. 5.18 Scanning electron micrographs of worn surface of UT under a load of 10 N load and at different speeds.

Figure 5.19 (a-d) shows the SEM images of the surface of CT7 worn at different speeds of 0.2, 0.8, 1.4, and 2.0 m/s under a constant load of 10N. All the micrographs show fine grooves in the direction of sliding along with the dimples. The dimples are visible initially at the lowest speed (Fig. 5.19 a) and gradually get completely filled with the debris until with increasing speed, as seen from Figs. 5.19 (b-d). A transfer layer of wear debris is observed to be present on the surfaces worn at sliding speeds of 1.4 and 2.0 m/s, as evident from Figs. 5.19 (c & d). Also, the transfer layer appears to have covered almost the entire area for the surface worn at a speed of 2.0 m/s, as seen from Fig. 5.19 (d). A significant deposition at the brim is also very clearly visible.

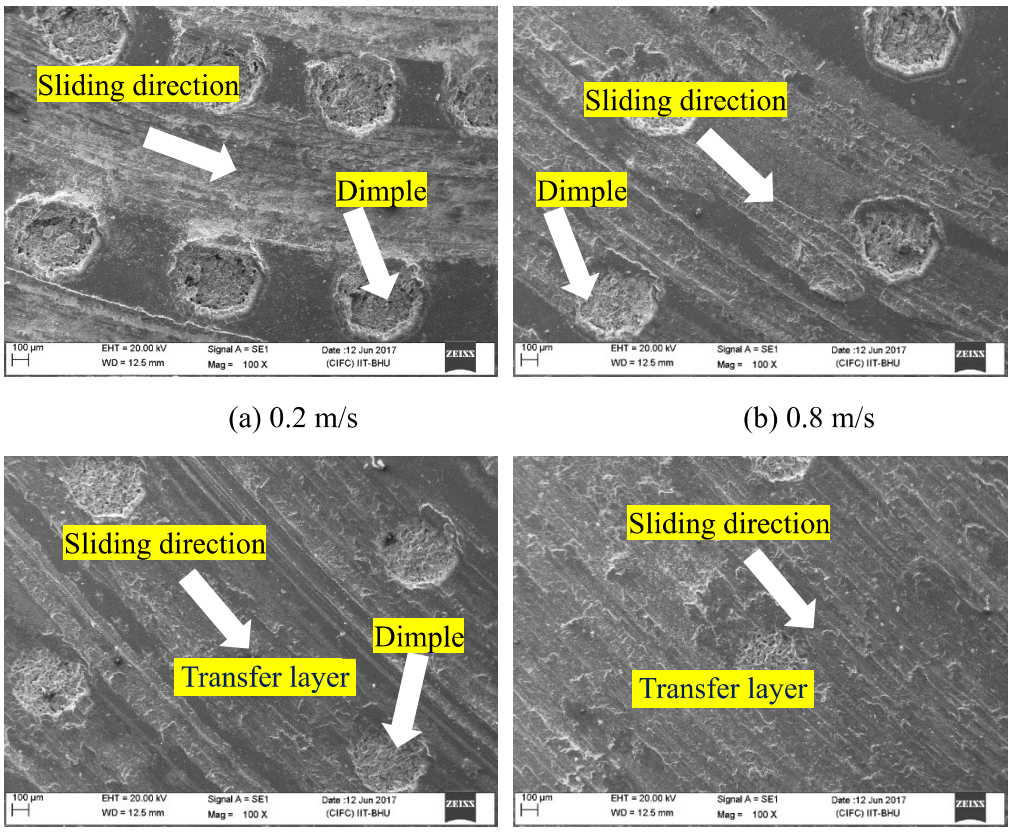

(a) 0.2 m/s (b) 0.8 m/s

(c) 1.4 m/s (d) 2.0 m/s

Fig. 5.19 Scanning electron micrographs of worn surface of CT7 under 10 N load and at different speeds.

Figure 5.20 (a-d) shows the worn surface morphologies of CT20 slid at different speeds of 0.2, 0.8, 1.4, and 2.0 m/s under a constant load of 10 N. The worn surfaces reveal the presence of fine grooves along with dimples which appear to be filled to a different extent based on the speed of sliding. The dimples are visible initially (Fig. 5.20 a) and gradually get filled with the debris to a different extent with increasing speed, as seen from Figs. 12 (b-d).

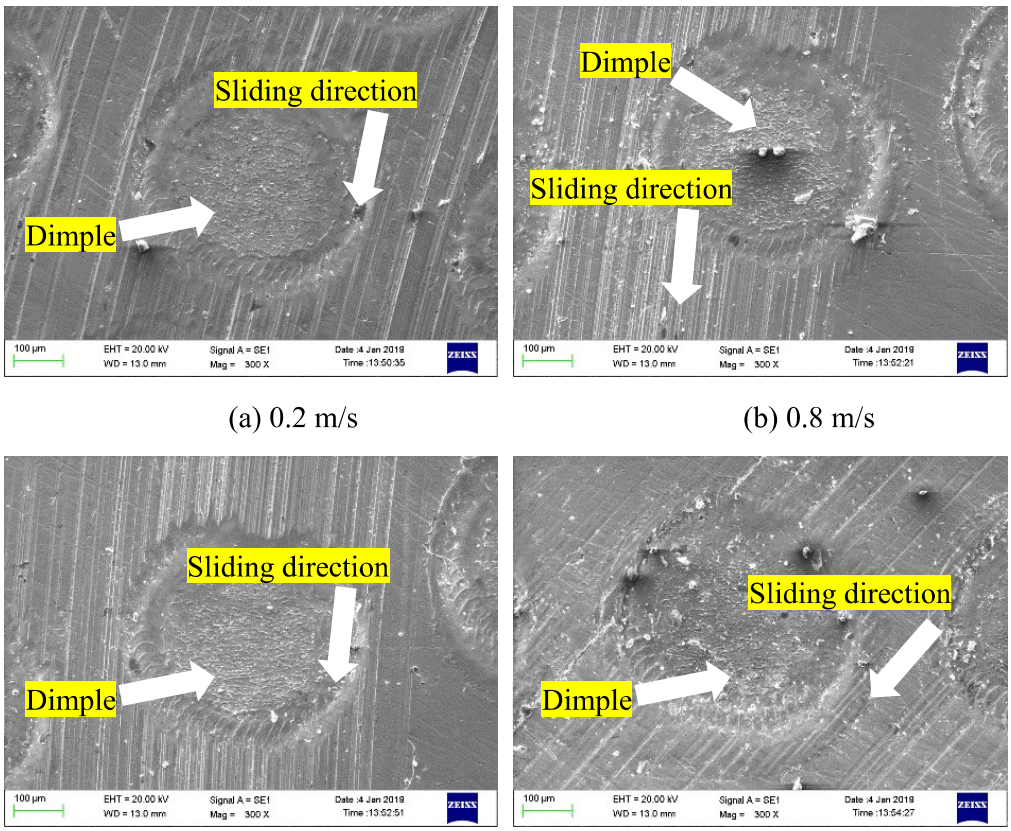

(a) 0.2 m/s (b) 0.8 m/s

(c) 1.4 m/s (d) 2.0 m/s

Fig. 5.20 Scanning electron micrographs of worn surface of CT20 under 10 N load and at different speeds.

Figure 5.21 (a-d) shows the SEM images of the surface of BT7 worn at different speeds of 0.2, 0.8, 1.4, and 2.0 m/s under a constant load of 10N. All the micrographs show fine grooves in the direction of sliding along with the dimples. The dimples are visible initially at the lowest speed of 0.2 m/s (Fig. 5.21 a) and gradually get completely filled with the debris with increasing speed as seen from Figs. 5.21 (b-d). A transfer layer of wear debris is observed to be present on the surfaces worn at sliding speeds of 1.4 and 2.0 m/s, as evident from Figs. 5.21 (c & d). In addition, the transfer layer appears to have covered almost the entire area for the surface worn at a speed of 2.0 m/s, as seen from Fig. 5.21 (d). The dimples may be seen clearly at relatively lower speeds but appear to have completely filled with the wear debris at

the highest speed of 2.0 m/s used in the study. A significant deposition at the brim is also very clearly visible.

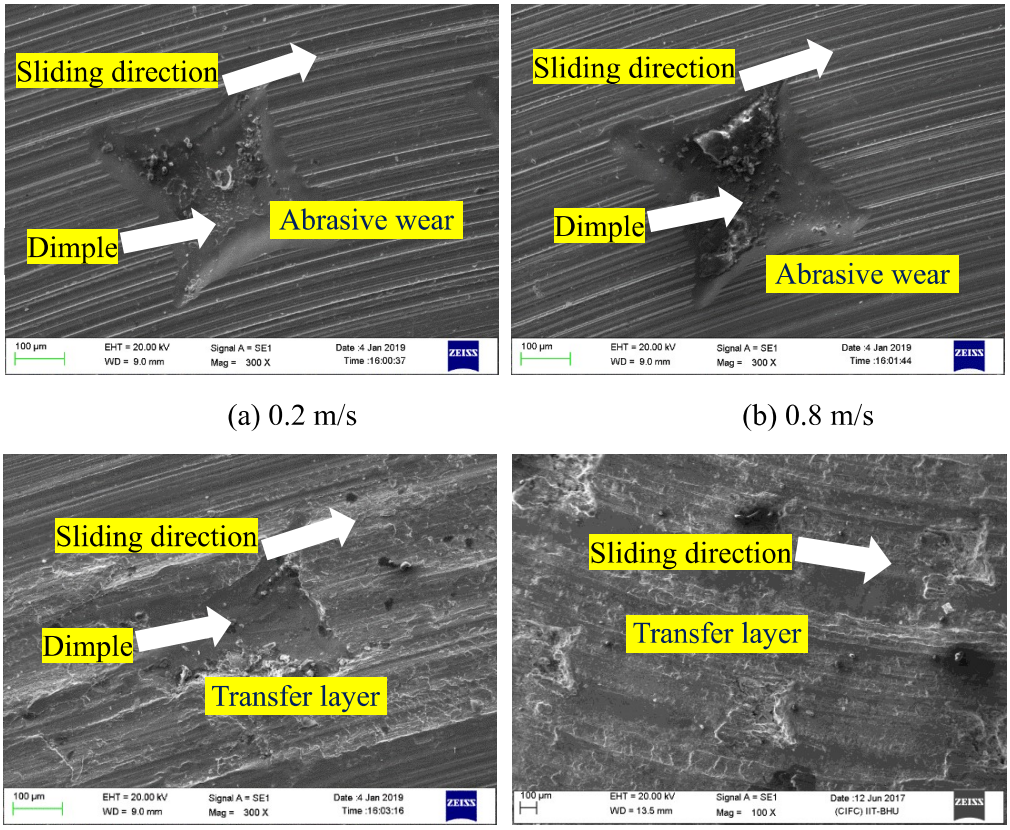

(a) 0.2 m/s (b) 0.8 m/s

(c) 1.4 m/s (d) 2.0 m/s

Fig. 5.21 Scanning electron micrographs of worn surface of BT7 under 10 N load and at different speeds.

The worn surface morphologies of BT20 slid at varied speeds of 0.2, 0.8, 1.4, and 2.0 m/s under a constant load of 10N are shown in Figs 5.22 (a-d). The dimples are evident at first (Fig. 5.22 a) and gradually get filled with the debris until these disappear, as shown in Figs. 5.22 (b-d). Fine grooves and differentially filled dimples can be seen on the worn surface corresponding to BT20, as shown in Fig 5.22.

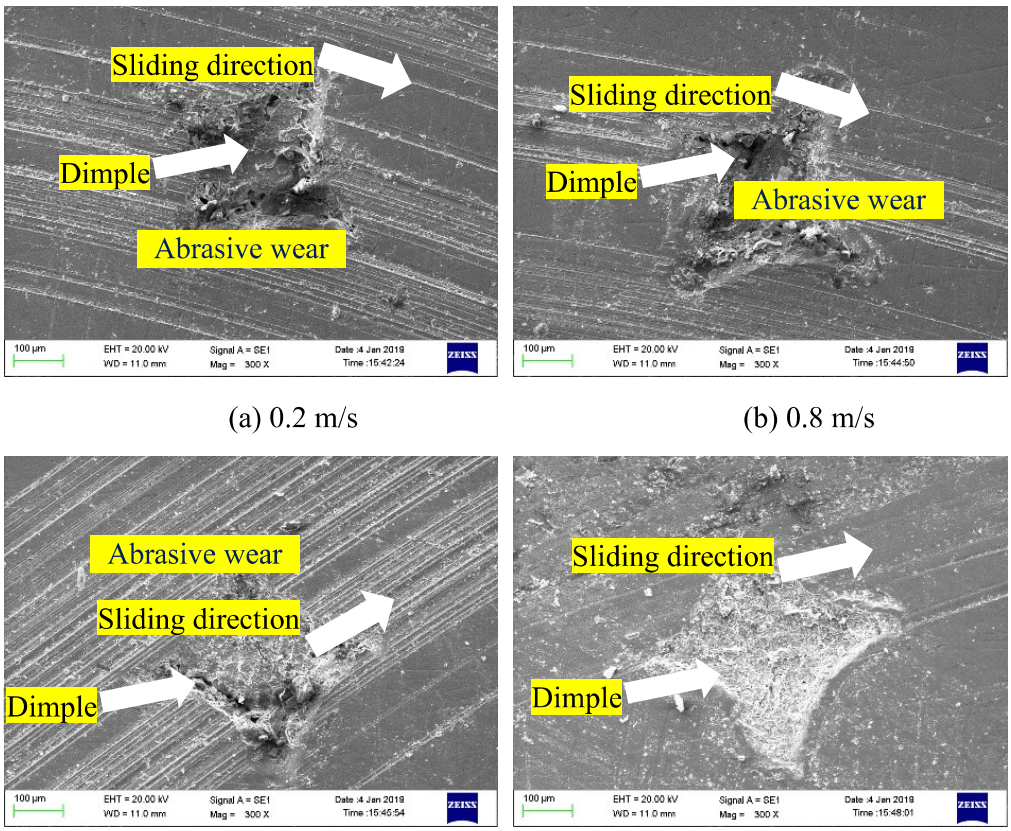

(a) 0.2 m/s (b) 0.8 m/s

(c) 1.4 m/s (d) 2.0 m/s

Fig. 5.22 Scanning electron micrographs of worn surface of BT20 under 10 N load and at different speeds.

The worn surfaces of UT steel slid at different speeds under a constant load of 30 N are shown in Figs. 5.23 (a-d). The SEM micrographs reveal grooves at 0.2 m/s and 0.8 m/s. However, at higher speeds of 1.4 m/s and 2 m/s, the grooves are barely seen, and surfaces seem to be covered with a transfer layer which appears to be torn at a few places indicating the occurrence of adhesion as evident from Figs 5.23 (c) and (d), respectively.

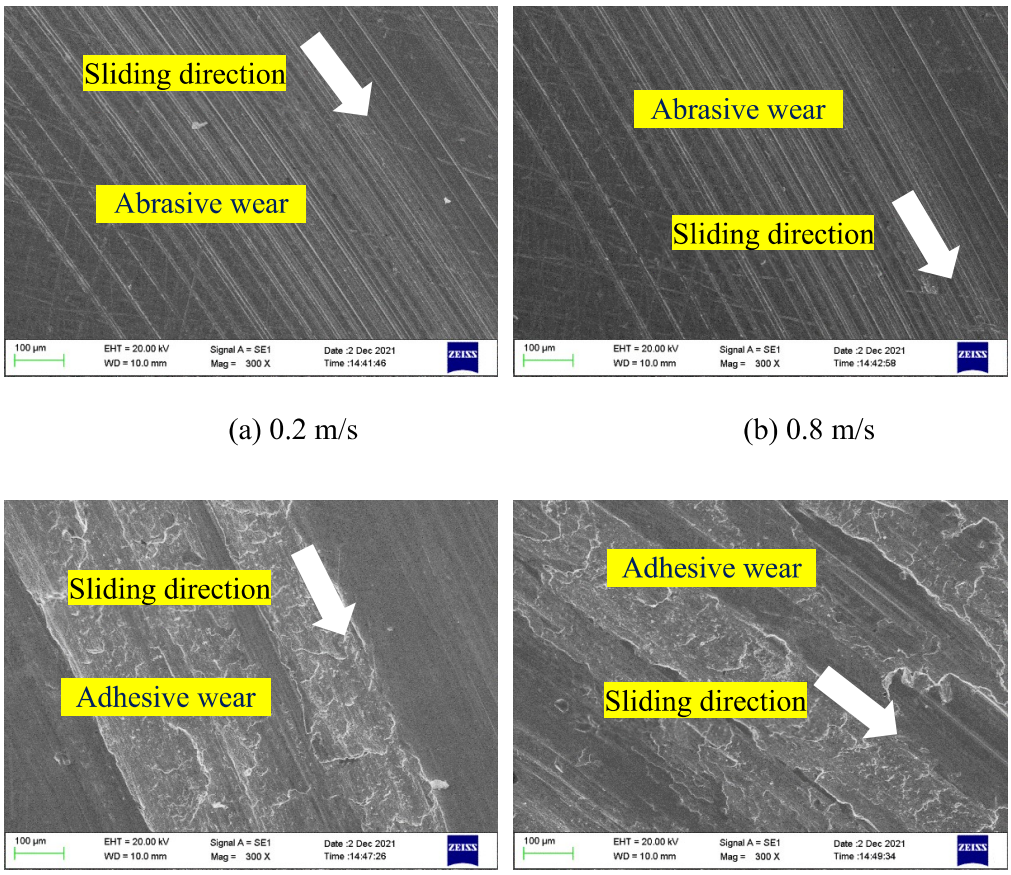

(a) 0.2 m/s (b) 0.8 m/s

(c) 1.4 m/s (d) 2.0 m/s

Fig. 5.23 Scanning electron micrographs of worn surface of UT under 30 N load and at different speeds.

Figure 5.24 (a-d) shows the SEM images of the surface of CT7 worn at different speeds of 0.2, 0.8, 1.4, and 2.0 m/s under a constant load of 30N. All the micrographs show the presence of fine grooves in the direction of sliding along with the dimples. The worn bulges at the brim of the dimples can be observed at all speeds. The micrographs suggest that the surfaces have no substantial wear loss, which is also evident from Fig. 5.12.

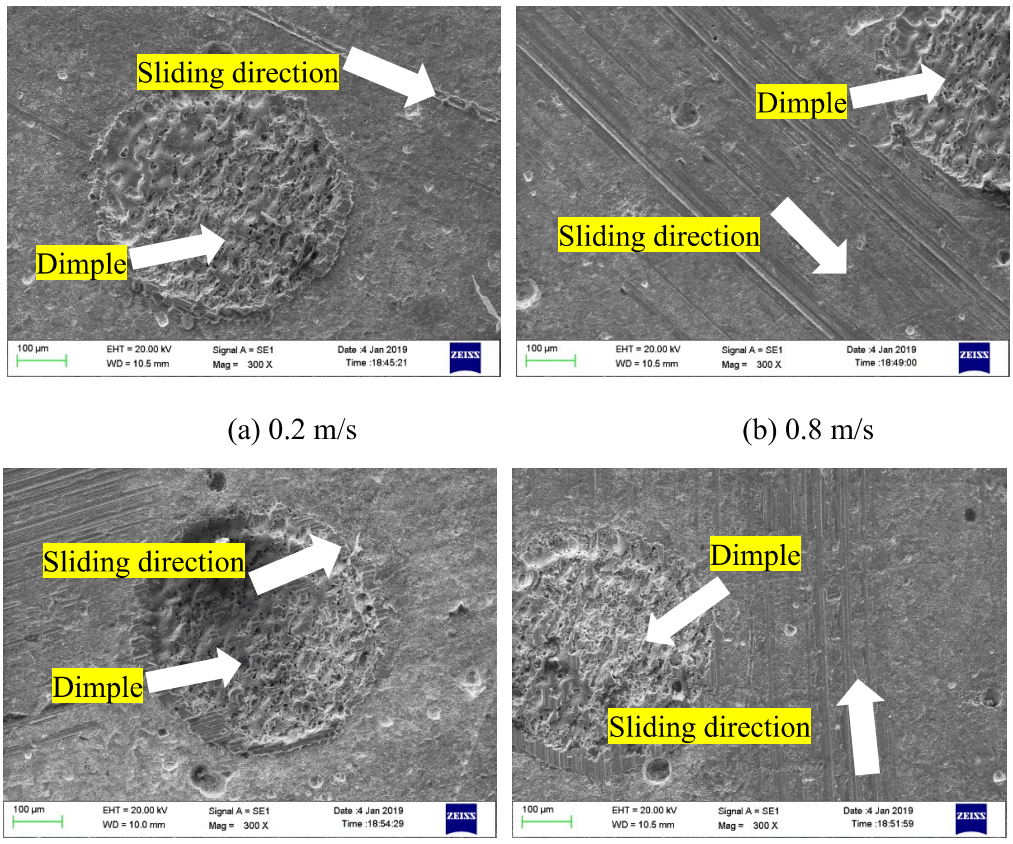

(a) 0.2 m/s (b) 0.8 m/s

(c) 1.4 m/s (d) 2.0 m/s

Fig. 5.24 Scanning electron micrographs of worn surface of CT7 under 30 N load and at different speeds.

SEM images of the surface of CT20 worn at different speeds of 0.2, 0.8, 1.4, and 2.0 m/s under a constant load of 30 N are shown in Figs. 5.25 (a-d). One may observe the presence of fine grooves along the direction of sliding along with the dimples. The worn bulges at the brim of the dimples are also visible at all speeds. The micrographs suggest that the surfaces exhibit a little amount of wear under single drop lubrication at this load and speed, which is also obvious in Fig. 5.12.

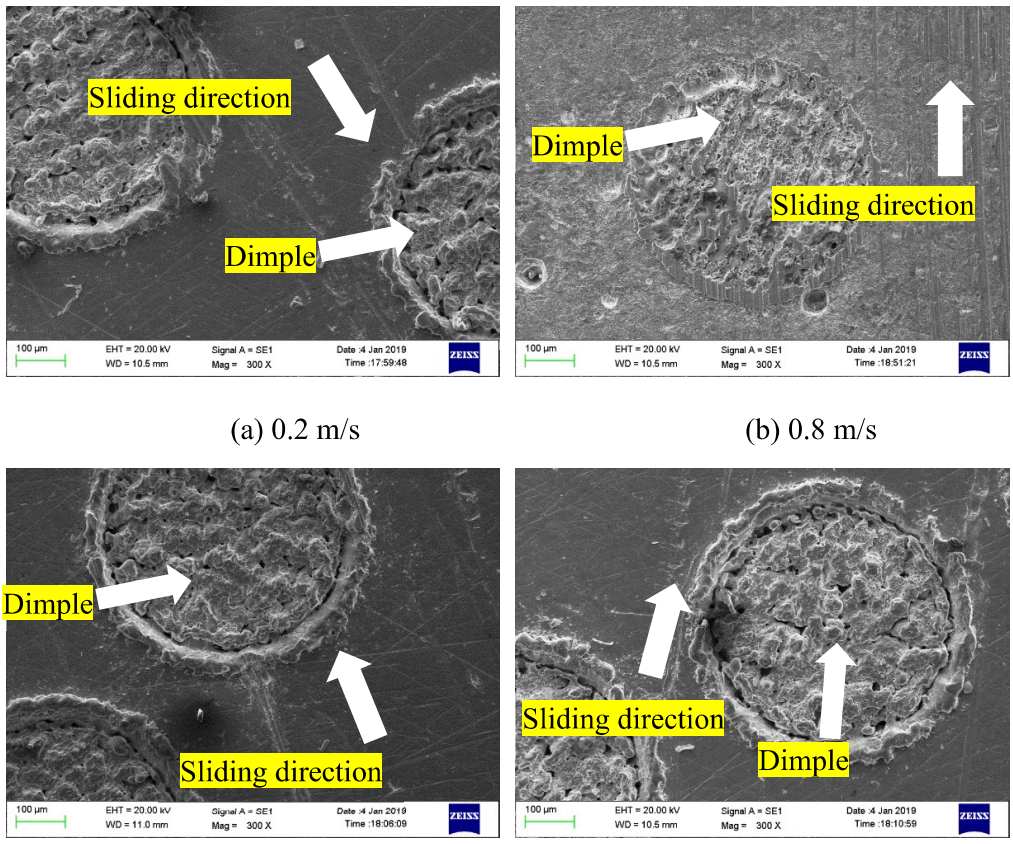

(a) 0.2 m/s (b) 0.8 m/s

(c) 1.4 m/s (d) 2.0 m/s

Fig. 5.25 Scanning electron micrographs of worn surface of CT20 under 30 N load and at different speeds.

Figure 5.26 (a-d) shows the SEM images of the surface of BT7 worn at different speeds of 0.2, 0.8, 1.4, and 2.0 m/s under a constant load of 30N. All the micrographs show the presence of very fine grooves along the sliding direction, which are more visible at relatively higher speeds of 1.4 and 2 m/s. The worn rim of the cavities can also be observed at all speeds. The micrographs indicate that under drop lubrication at this load and speeds, the surfaces have undergone negligible wear as seen from Fig. 5.12 also. SEM images of the surface of BT20 worn under a constant load of 30 N and at different speeds are presented in Figs. 5.27 (a-d). At all speeds, fine grooves can be observed along the worn track. Furthermore, bulges at the brim of the dimples show deformation at all speeds.

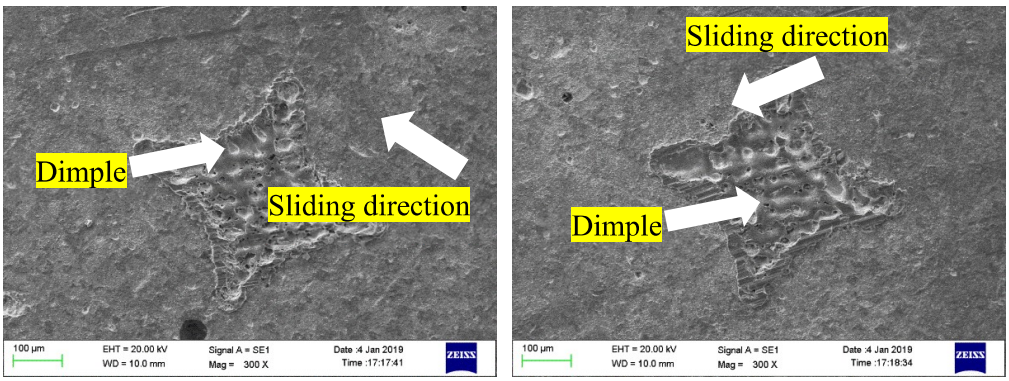

(a) 0.2 m/s (b) 0.8 m/s

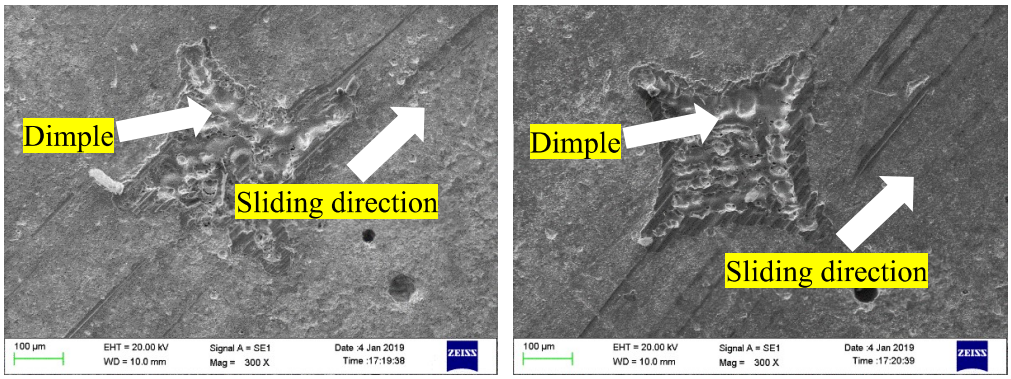

(c) 1.4 m/s (d) 2.0 m/s

Fig. 5.26 Scanning electron micrographs of worn surface of BT7 under 30 N load and at different speeds

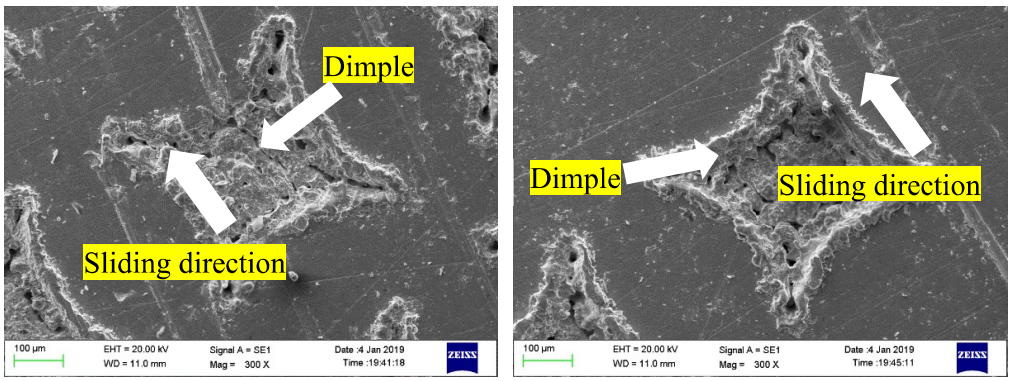

(a) 0.2 m/s (b) 0.8 m/s

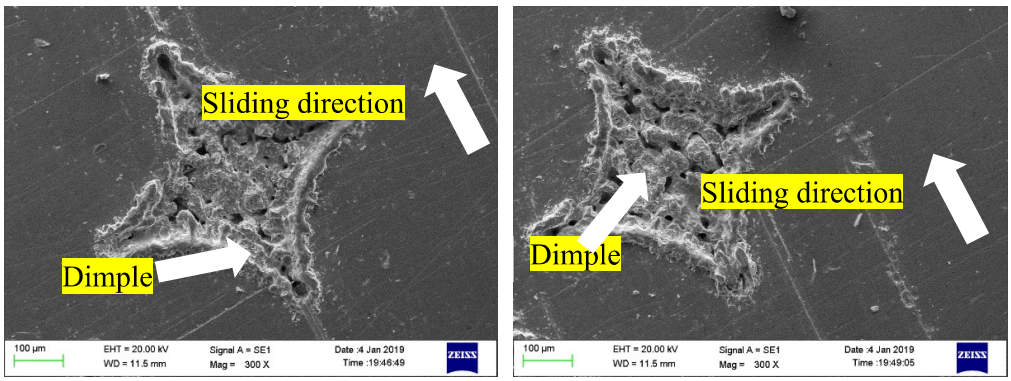

(c) 1.4 m/s (d) 2.0 m/s

Fig. 5.27 Scanning electron micrographs of worn surface of BT20 under 30 N load and at different speeds.

SEM micrographs of the worn surface of the UT at different speeds under single drop lubrication and at a constant load of 50 N are shown in Fig. 5.28. The worn surface of the untextured specimen shows a typical morphology of a worn steel surface with the presence of wear marks along the sliding direction. At all the speeds under 50 N load, the surfaces show signs of adhesion and subsequent removal of material which might have been responsible for higher wear of UT compared to the textured as seen from Fig. 5.13. one may observe the severity of adhesion with increasing speed from 0.2 to 2.0 m/s.

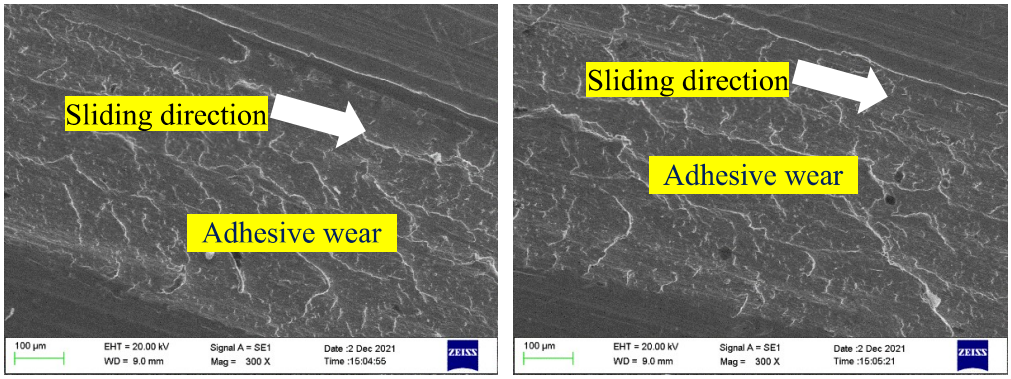

(a) 0.2 m/s (b) 0.8 m/s

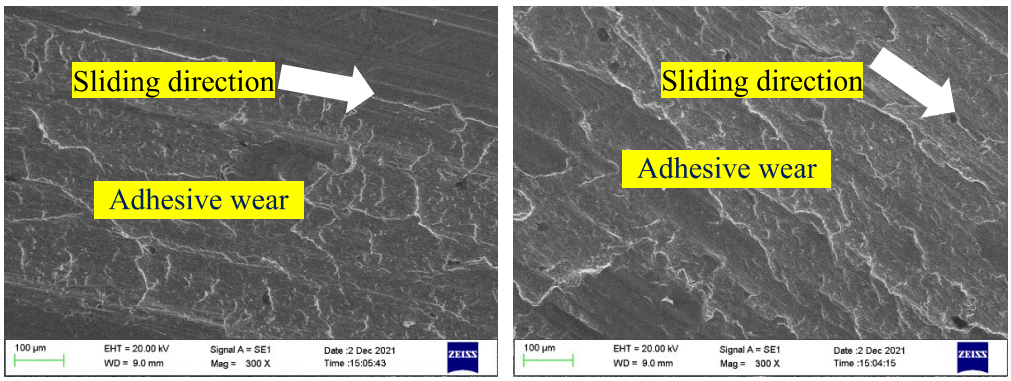

(c) 1.4 m/s (d) 2.0 m/s

Fig. 5.28 Scanning electron micrographs of worn surface of UT under 50 N load and at different speeds.

Figure 5.29 (a-d) shows SEM images of CT7 at different speeds under a constant load of 50 N and in single drop lubrication. The surfaces of the specimen show grooves and traces of adhesive wear. At 0.2 m/s, the surface reveals grooves, which are most likely caused by worn particles trapped under the contact with the sliding surface, along with the dimples that appear to have filled with debris as seen from Fig. 5.29 (a). The surface worn at a speed of 0.8 m/s (Fig. 5.28 b) reveals the presence of loose debris particles, a transfer layer of wear debris which is loosely bound at a few places and well compacted at other locations along with the filled dimple. The frictional heating might have resulted in the formation of a compacted layer of debris on the surface. At higher speeds of 1.4 and 2.0 m/s, the dimple appears to have filled completely, and the surfaces exhibit the presence of a compacted transfer layer of debris along with some loose wear debris particles as seen from Figs. 5.29 (c) and (d). however, the degree of compaction and the area covered by the transfer layer appears to be more at 2.0 m/s.

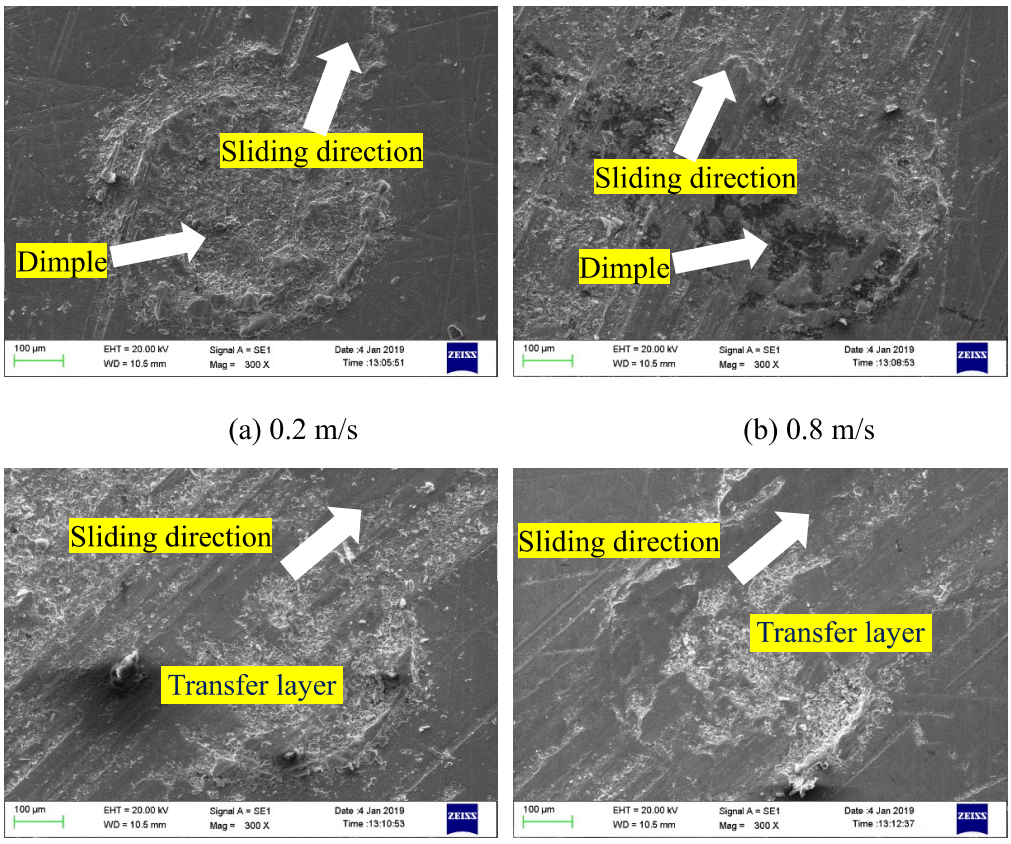

(a) 0.2 m/s (b) 0.8 m/s

(c) 1.4 m/s (d) 2.0 m/s

Fig. 5.29 Scanning electron micrographs of worn surface of CT7 under 50 N load and at different speeds.

The scanning electron micrographs of the worn surface of CT20 under a constant load of 50 N and at different speeds are shown in Fig. 5.30. At 0.2 m/s, the surface has fine grooves running along the direction of sliding, and the presence of debris is also seen in the dimple. As the speed increases to 1.4 m/s, the presence of grooves is reduced, however, the dimple appears to have filled with debris, however, a small unfilled patch may also be observed inside the dimple as shown in Fig. 5.30 (b). The grooves are barely discernible as the speed increased to 1.4 m/s and 2 m/s (Figs. 5.30 c and d)).

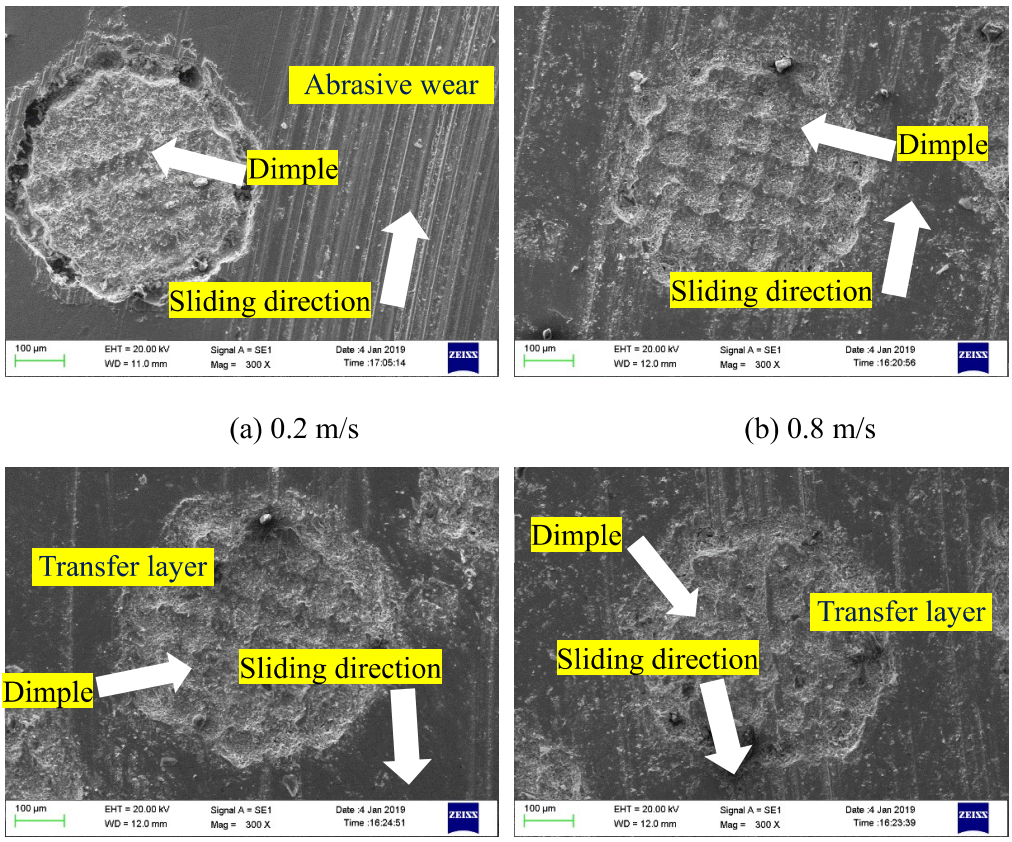

(a) 0.2 m/s (b) 0.8 m/s

(c) 1.4 m/s (d) 2.0 m/s

Fig. 5.30 Scanning electron micrographs of worn surface of CT20 under 50 N load and at different speeds.

Figure 5.31 shows the scanning electron micrographs of the worn surface of BT7 under a constant load of 50 N and at different speeds. At 0.2 m/s, the microgrooves can be observed along the direction of sliding, and worn particles seem to have filled the dimples as shown in Fig. 5.31 (a). The surface worn at a speed of 0.8 m/s reveals the existence of fine grooves all over the surface, along with the presence of debris particles in the dimple. As the speed increases to 1.4 m/s, the surface appears to have wider grooves indicating the occurrence of plastic deformation probably due to the softening caused by the frictional heating along with the presence of a smooth transfer layer. Also, the dimple appears to be partially filled with worn particles. At the highest speed of 2 m/s, the worn surface shows the presence of a loosely

bound transfer layer of debris which appears to be covering the larger area. The dimple is visible, but the debris appears to be obscuring it (Fig. 5.31 d).

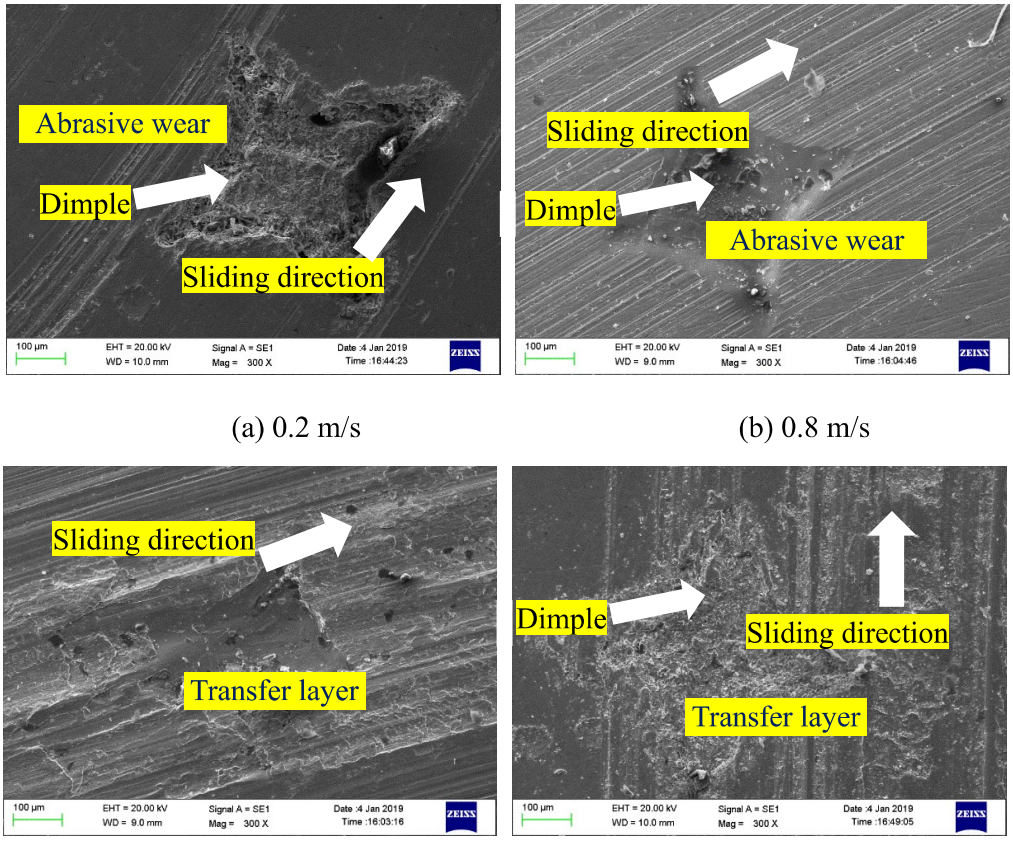

(a) 0.2 m/s (b) 0.8 m/s

(c) 1.4 m/s (d) 2.0 m/s

Fig. 5.31 Scanning electron micrographs of worn surface of BT7 under 50 N load and at different speeds.

The scanning electron micrographs of the worn surface of BT20 under a constant load of 50 N and at different speeds are given in Fig. 5.32. One may observe the presence of fine grooves along the sliding direction and the debris particles in the dimple on the surface worn at a speed of 0.2 m./s (Fig. 5.32 a). The surface worn at a speed of 0.8 m/s reveals the presence of fine wear marks and loose wear particles over the surface as well as in the dimple as seen from Fig. 5.32 (b) indicating the occurrence of abrasion by the loose wear particles. Similar features may also be observed on the surface worn at a speed of 1.4 m/s as seen from Fig. 5.32

(c). The worn particles appear to have filled the dimples as well. At 2 m/s, the surface shows the presence of a transfer layer of wear debris along with the wear marks from where the layer might have been detached as seen from Fig. 5.32 (d). One may also observe the presence of loose wear debris on the worn surface along with the dimple filled almost completely by the wear particles.

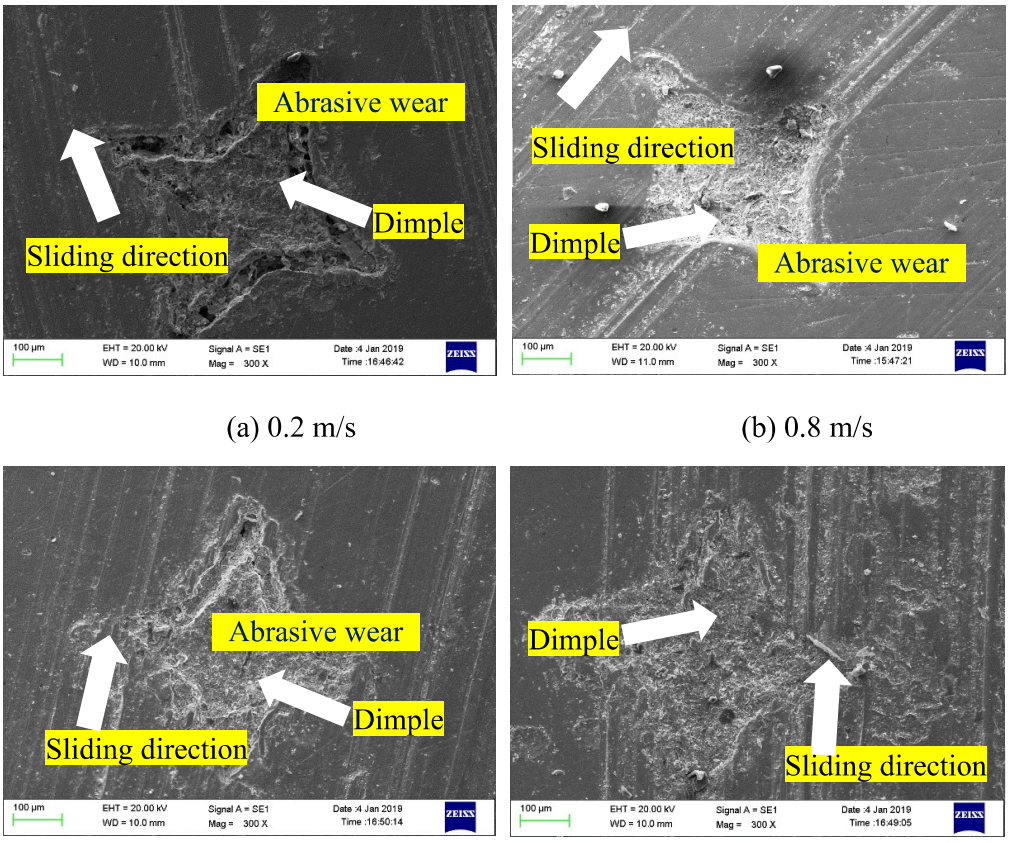

(a) 0.2 m/s (b) 0.8 m/s

(c) 1.4 m/s (d) 2.0 m/s

Fig. 5.32 Scanning electron micrographs of worn surface of BT20 under 50 N load and at different speeds.

Figure 5.33 shows SEM-EDS of the worn surface of BT7 at a constant load of 10 N and speed of 1.4 m/s which reveals the presence of oxygen over the surface indicating that the transfer layer is composed of some oxides of iron.

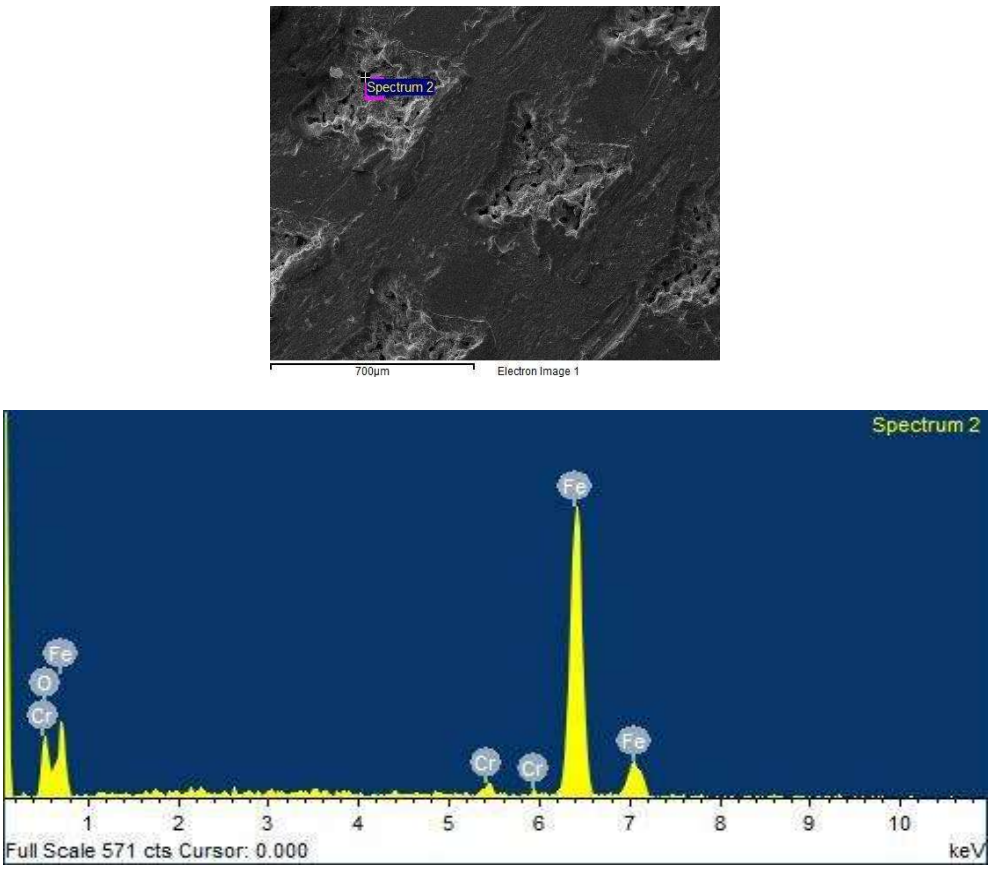

Fig. 5.33 SEM-EDS of worn surface of BT7 at a constant load of 10 N and sped of 1.4 m/s

Figure 5.34 shows the worn track and depth of a dimple (before and after the test) for BT7 tested at 0.8 m/s under a constant load of 10N in single drop lubrication. Figure 5.34 (a) depicts the 2D image of a bi-triangular dimple, whereas 5.34 (b) shows an analysis of the worn surface on the same track. The change in the depth before and after the tests can be clearly observed.

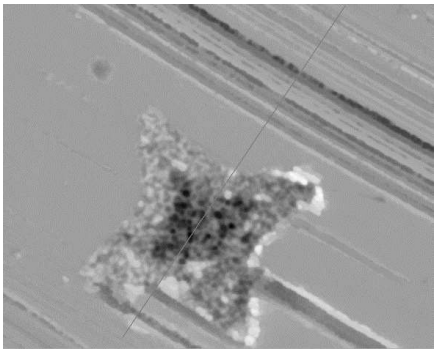

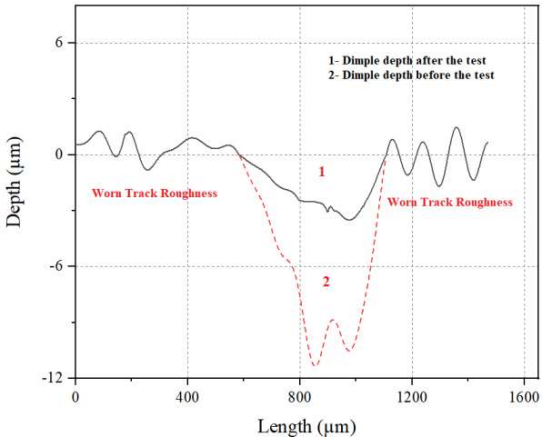

(a) Optical profilometer 2D image of a bi-triangular dimple and worn surface

(b) Worn surface analysis

Fig. 5.34 Worn track and depth of a dimple (before and after the test) for BT7 tested at 0.8 m/s under 10N load

The 3D morphologies of BT7 before and after the test at 0.2 m/s are presented in Figs. 5.35 (a) and (b), respectively. One may observe the depth of dimples ~ 8 µm before the test is performed and bulges at the brim of the dimple, as stated earlier (Fig. 5.35 a). However, the brims almost disappeared, and the depth also gets reduced due to the filling of the worn particles, as seen from Fig. 5.35 (b). One may also notice a worn track in the same area.

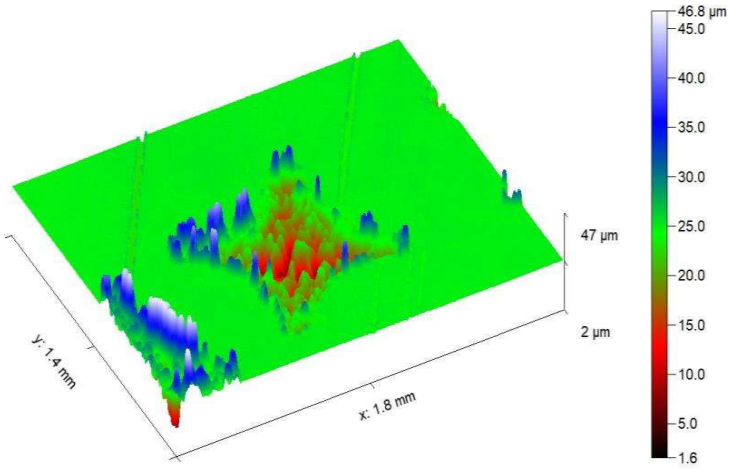

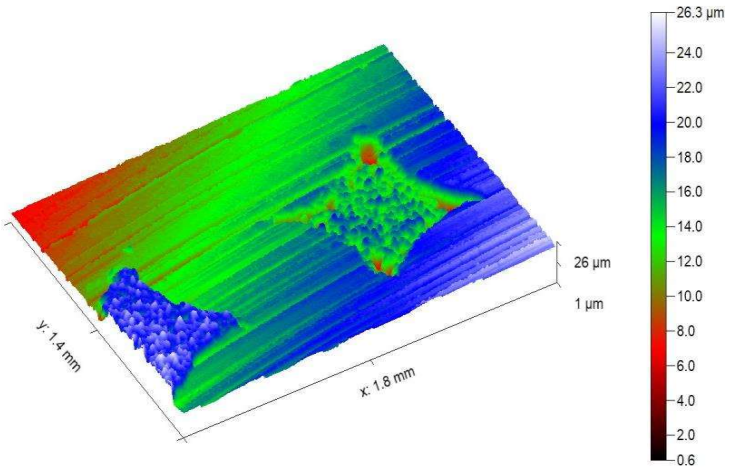

Fig. 5.35 3D Optical profilometry of BT7 slid at a load of 10 N at 0.2 m/s before (a) and after the test (b)

In order to determine the duration (number of cycles) of the effectiveness of dimples, tests for longer runs were carried out for CT20 at different speeds, and a sudden increase in the coefficient of friction has been considered as the effective lifetime of the dimples. The variation of coefficient of friction with the number of cycles for CT20 has been depicted in Fig. 5.36. At 0.2 m/s, an increase in the coefficient of friction can be observed for 14000 revolutions, whereas the same occurs after 8000 revolutions at 0.8 m/s. However, the coefficient of friction has been observed to increase after 14000 revolutions at 1.4 m/s. At 2 m/s, the change can be observed after 10000 revolutions. The increase in the coefficient of friction after a certain number of revolutions indicates the loss in effectiveness of the dimples.

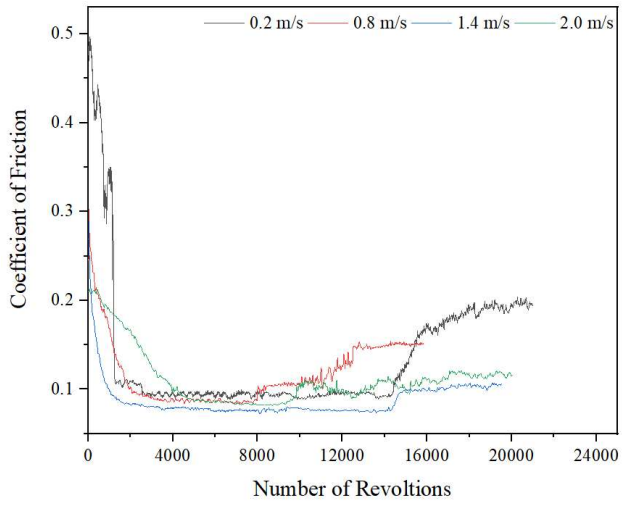

Fig. 5.36 Variation of coefficient of friction for CT20 for a maximum number of revolutions at different speeds and 10N load.

5.2 LUBRICATION REGIMES

The influence of textures on the tribological performance of the system in a limited supply of lubricant shows a combination of lubrication regimes based on characteristics of textures (shape, size, density), applied loads, and speeds. Figures 5.37, 5.38, and 5.39 depict the lubrication regimes based on the observed average coefficient of friction as suggested by Wen and Huang (2012).

Figures 5.37 (a-d) show the average coefficient of friction and lubrication mechanisms for UT and textured samples at various sliding speeds and a constant load of 10 N under single drop lubrication. UT shows a boundary lubrication regime for all the speeds at this load. The specimen having bi-triangular dimples with 20% density i.e., BT20 falls under a boundary lubrication regime, whereas, BT7 with 7% density is found to remain in the regime of mixed lubrication at all the speeds used in the present study. The specimen with 7% circular dimples i.e., CT7 is observed to be in a mixed lubrication regime at the speeds of 0.8 and 1.4 m/s, whereas, at 0.2 m/s and 2 m/s CT7 remains in a boundary lubrication regime. CT20 has been

observed to be in the mixed lubrication regime at 1.4 m/s, whereas a regime of boundary lubrication appears to have prevailed at the speeds of 0.2, 0.8 and 2 m/s.

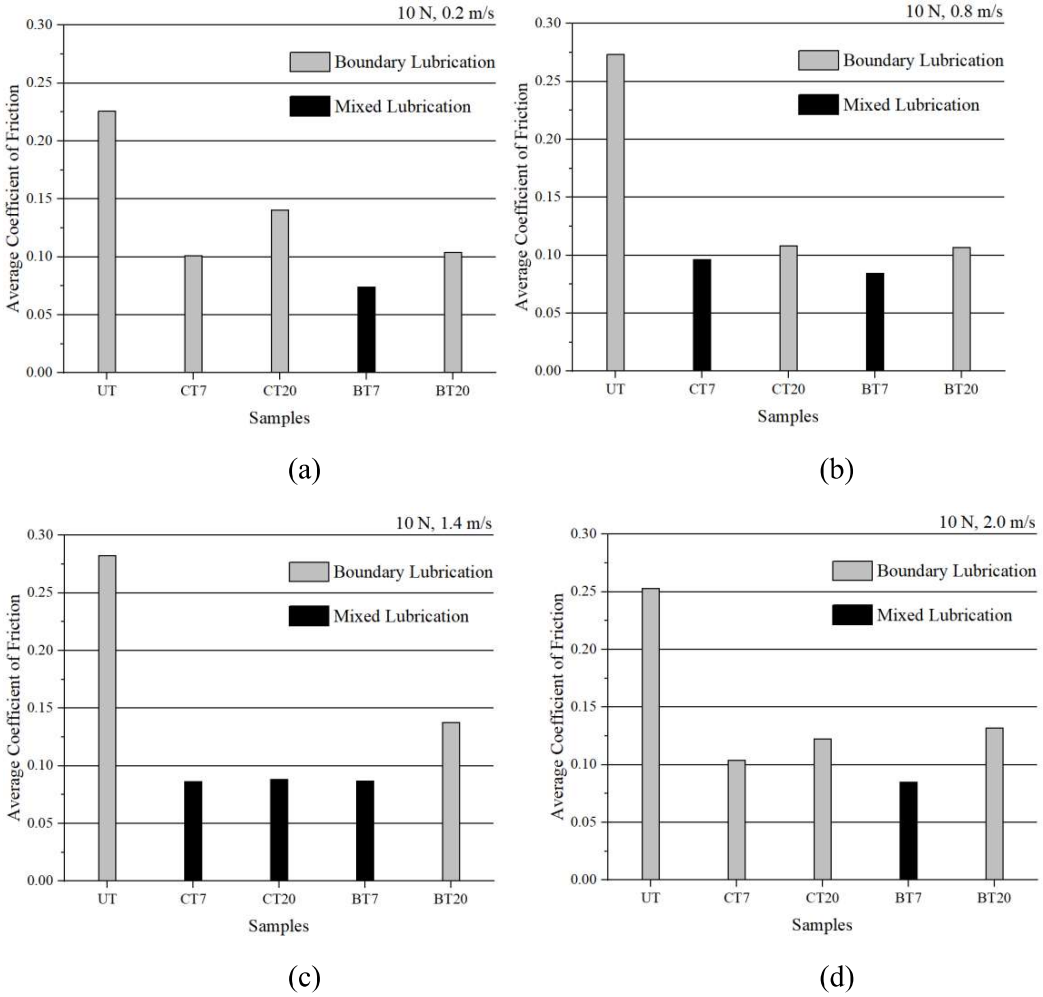

Fig. 5.37 Average coefficient of friction of discs at various sliding speeds, 10 N load in single drop lubrication.

Figures 5.38 (a-d) depict the average coefficient of friction for UT and textured samples in single drop lubrication at different sliding speeds and a constant load of 30 N. Based on the observed coefficients of friction, all the textured specimens are found be in a mixed regime of lubrication for all the speeds whereas untextured specimen is observed to be in a regime of boundary lubrication.

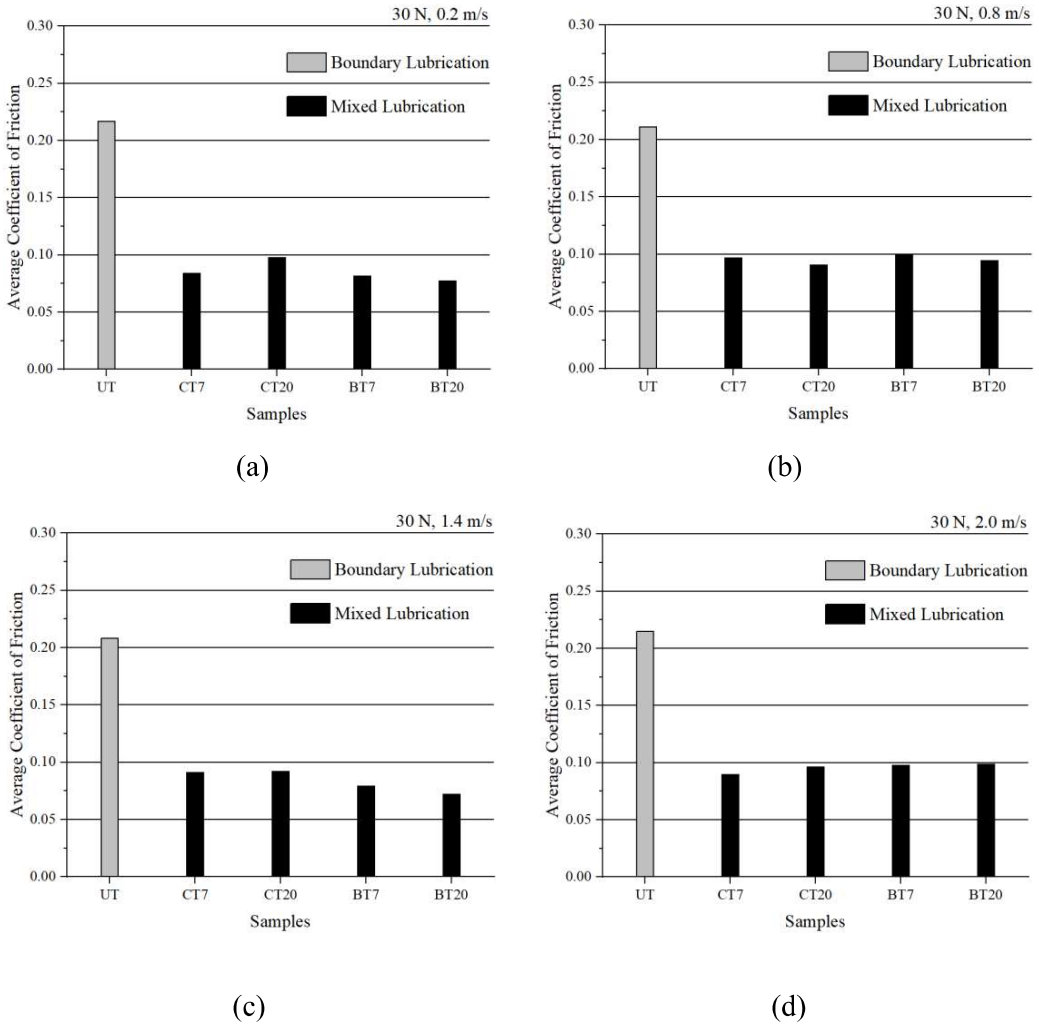

Fig. 5.38 Average coefficient of friction of discs at various sliding speeds, 30 N load in single drop lubrication.

The average coefficient of friction for various samples at different speeds under a constant load of 50 N is shown in Fig. 5.39 (a-d). A boundary lubrication regime is observed for all the samples for most of the operating conditions. However, BT7 is found to remain in a regime of boundary lubrication at relatively lower speeds of 0.2 and 0.8 m/s which changes to a mixed regime of lubrication at higher speeds of 1.4 and 2.0 m/s. CT20 is also observed to be in a regime of mixed lubrication at the highest speed of 2 m/s used in the present study.

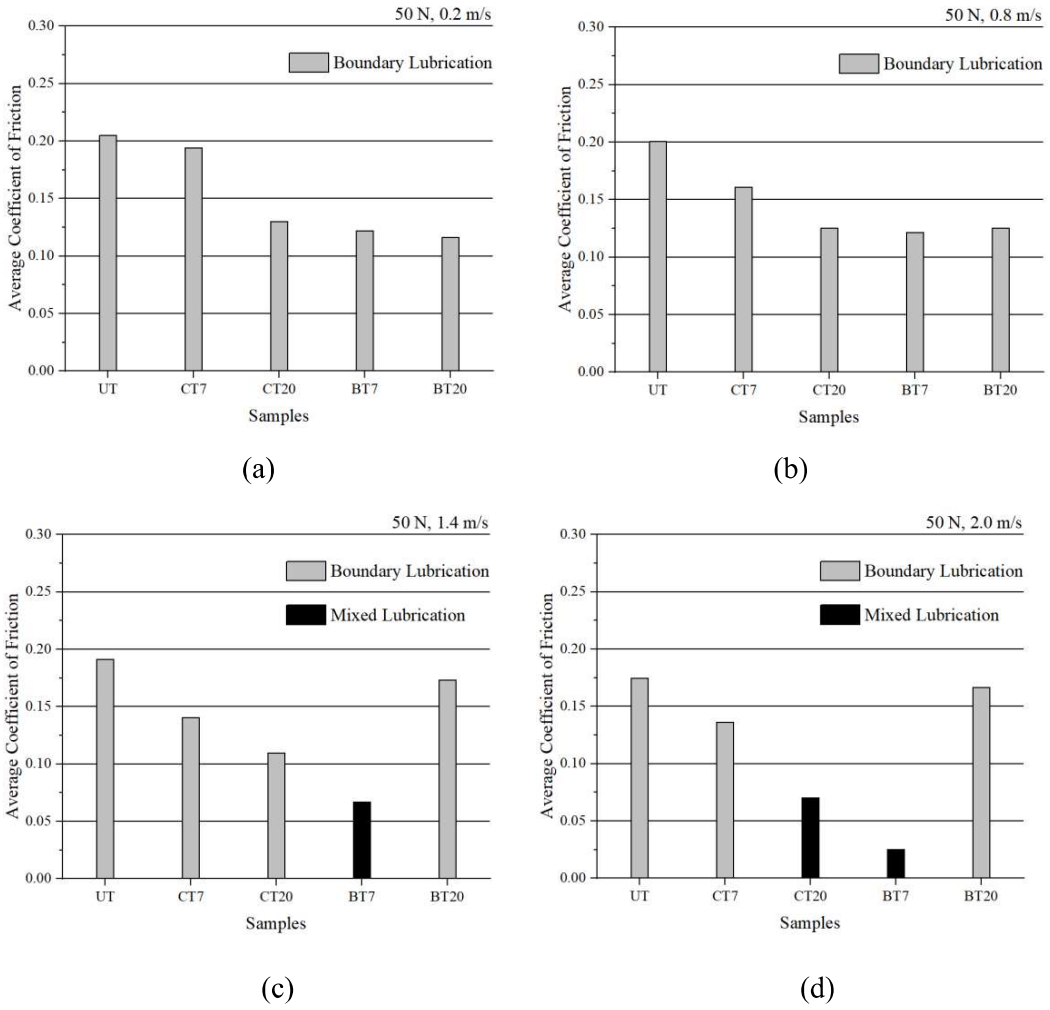

Fig. 5.39 Average coefficient of friction of discs at various sliding speeds, 50 N load in single drop lubrication.

5.3 DISCUSSION

The tribological behaviour for the textured surfaces under lubricated conditions may be explained on the basis of the pressure build-up in the presence of lubrication. An up-thrust to the contacting parts, as it moves over the textured region, results in the separation of two mating bodies and hence, a reduction in the extent of surface contact. However, the presence of this lifting effect depends on the density of dimples. Moreover, at different loads and speeds, the shape of the dimples also plays a major role in governing the relative magnitude of the pressure peak (high lubrication film pressure) and pressure trough (low lubrication film

pressure), which allows the determination of the magnitude of up-thrust/lift. Also, there is a possibility of adhesion between contacting materials and the generation of wear debris due to rubbing action under the limited supply of the lubricant, which may also affect the performance of the textured specimen.

Textural patterns have been found to increase friction and even cause the lubricating film to collapse under higher loads and/or lower speeds. Low loading and/or high speed, on the other hand, are favourable conditions for textured surfaces to exert hydrodynamic action. Different lubrication mechanisms exist depending on the shape, depth, and density of the surface texture pattern. Surface texture designs that are successful in one regime may not be successful in another. The textural design having large and shallow dimples, which provide hydrodynamic lift ideally under low load and high-speed situations, shows benefit in mixed and/or boundary lubrication regimes in a limited supply of the lubricant, as indicated by Hsu et al., (2016). In the present study, the tribological performance of bearing steel having circular and bi-triangular dimples with two distinct densities, i.e., 7% and 20%, has been evaluated under different sliding speeds (0.2, 0.8, 1.4, and 2.0 m/s) and normal loads of (10, 30, and 50 N) under single drop lubrication. The regimes of lubrication for different specimens have been identified based on their observed coefficient of friction, as suggested by Wen and Huang (2012).

Under a load of 10 N, the untextured specimens show a higher value of the coefficient of friction compared to the textured one. The lubricant added to the sliding surface form a boundary lubricated film during the revolutions. The abrasive wear of the surface is caused by the worn particles while sliding, as shown by clearly visible parallel scratches and abrasive grooves in the sliding direction (Fig. 5.18 a-d). As the sliding speed increases, the lubrication becomes more efficient, and the wear rate reduces, as shown in Fig. 5.3 (c). However, the coefficient of friction at 0.8 m/s and 1.4 m/s shows an increase in the coefficient of friction

before decreasing again at 2 m/s. This unusual increase may be caused due to presence of worn particles under the contact surface.

The lower coefficient of friction for BT7 and CT7 at a speed of 0.2 m/s may also be explained on the basis of the worn surface morphologies shown in Fig. 5.19 (a) and 5.21 (a), which indicate the possible presence of micro-bearings during the test and gradual filling of dimples by worn particles with increasing speed. The loose wear particles appear due to initial wear caused by wearing of bulges which might have initiated abrasion (5.21 a). After the loose wear particles are trapped inside the cavity, the film becomes effective. However, the fluctuating behaviour of the coefficient of friction (Fig. 5.1 d) shows the instability of the film. This indicates the presence of the stick-slip phenomenon. CT7 shows a similar behaviour, however, the grooves are not visible (Fig. 5.19 a), as in the case of BT7. This indicates less effectiveness of circular dimples in capturing worn particles and rubbing of the pin on the disc surface (Fig. 5.11). The film is unstable at this load and speed, giving oscillating behaviour of the friction curve (Fig. 5.1 b).

An increased coefficient of friction for CT7, BT7, and BT20 corresponding to a speed of 2.0 m/s may be due to the significant filling of dimples, as reflected in Fig.5.21 (a, b) for BT7 and complete filling of dimples for BT7 and CT7 without any visible dimples, as seen from Figs. 5.19 (d) and 5.21 (d) and the possibility of disappearing dimples and the micro-bearing effect. The same can be seen for BT20 in Fig. 5.22 and for CT20 in Fig. 5.20. The absence of loose wear particles at the sliding interface may have helped in smooth sliding by avoiding abrasive action thereby, reducing the coefficient of friction. The wear rate is observed to be relatively high for BT7, BT20, CT7, and CT20 at the lowest speed of 0.2 m/s, but it decreases and becomes minimum at the maximum speed of 2.0 m/s for BT7, BT20, and CT7. However, the wear rate is observed to increase slightly for CT20 at 2.0 m/s. This may be attributed to the presence of wear particles and the efficiency of dimples as a trap of worn

particles, which can be judged from Figs. 5.19, 5.20, 5.21, and 5.22, where dimples seem to have been filled to different extents depending on the speed, shape, and density of dimples. At a relatively lower speed of 0.2 m/s, initial wear is high due to wearing out of bulges at the brim. The number of dimples per unit area is more on the surface with higher area density, increasing thus the possibility of the generation of more wear particles. The different behaviour of BT20 may be due to the presence of a higher number of dimples and larger size of bulges which could be seen in Fig. 4.3 (a) for bi-triangular dimples. The dimples get completely filled (Figs. 5.19-5.22 (b, c, d)) due to the generation of more wear debris with increasing speed from 0.2 to 1.4 m/s. However, a further increase in speed to 2.0 m/s causes a decrease in the wear rate of BT20 as seen from Fig. 5.11, due to the complete filling of dimples.

As shown in Figs. 5.19 & 5.21, abrasion and adhesion can also be observed from the morphology of the worn surface for 7% dimple density. It is clearly seen that bi-triangular texture shows better surface characteristics (Figs. 5.21 a, b) in comparison to the circular texture (Figs. 5.19 a, b). As the density increases to 20%, the wearing effect is not the same, especially in the case of BT20 (Figs. 5.22 b, c). BT7 shows possible film formation, which helps in the reduction of friction and wear at all the speeds under 10 N load, as indicated in Figs. 5.37 (a-d). At medium speeds of 0.8 m/s and 1.4 m/s, circular dimples with 7% density (CT7) become effective for film formation in mixed lubrication, thus a reduced value of average coefficient of friction and the wear rate. Circular dimples with a 20% dimple density (CT20) show bearing action at 1.4 m/s under a 10 N load. These results indicate that dimples affect the wear rate, but the effect is minor due to their limited numbers. For a longer run, as the dimples get filled gradually, it becomes difficult for them to trap more debris and retain lubricant as well. The result suggests that BT7 having bi-triangular dimples with 7% density, has the optimum performance under 10 N load and the speeds used in the current study.

In one drop lubrication, as the test proceeds, the oil exhausts after a certain number of revolutions and direct contact occurs, causing the wear of surface at the track. The entrapment of wear debris in the dimples reduces the depth and ability of dimples to act as micro-bearing. Once the oil exhausts after a certain number of revolutions, surface wears out and the roughness of the surface increases. Figure 5.34 (b) shows that at the end of the test, depth of the roughness (R_a= 0.89 µm) is very less in comparison to the dimple's initial depth (8 µm), and the quantity of oil as the test proceeds and roughness appears, is not adequate for the roughness to act as micro-bearing. Hence, the effect of roughness in comparison to the dimples may not be prominent in the present study.

3D optical profilometry of BT7 (Fig. 5.35) shows small bumps of the material on the inside edge of the texture as a by-product of laser ablation are indicated as spikes in the plots of the surface profilometer (Fig. 5.35 a), which disappear after the test (Fig. 5.35 b). At a certain speed, as the dimples start filling, the lubricant film breaks down, leading to failure lubrication. This results in a significant increase in the area of contact between the mating materials leading to the generation of large frictional heat and subsequent adhesion. Additionally, the particles generated through adhesive wear scratch the surface further and result in much wider and deeper grooves. (K. Li et al., 2014)

In the study under 10 N load, the coefficient of friction for CT7 ranges from 0.086 to 0.10, indicating that the lubrication regime is defined by boundary and mixed lubrication. On the other hand, CT20 has a coefficient of friction between 0.088 to 0.14, indicating a mixed and boundary lubrication regime. As far as BT7 is concerned, the coefficient of friction lies between 0.074 to 0.086, indicating that the regime of lubrication is mixed at lower speed which changes to EHL at higher speeds. However, BT20 exhibited a boundary lubrication regime with coefficients of friction lying between 0.10 to 0.137 for all the speeds used in the present study. It reflects that the generation of the micro-bearing effect depends on the shape of the

dimples and ceases for 20% density of bi-triangular shape at the speed used in the current investigation. Also, the value of the coefficient of friction for all the samples remained lower till the end of the test. Hence, it may be concluded that the oil film remains intact during the friction test for the given number of revolutions.

In the study under 30 N load, the textured surfaces have shown the coefficient of friction and wear to be lower than when tested under 10 N load (Fig. 7-10), with some exceptions seen at 0.8m/s (Fig. 5.8). The average coefficient of friction for untextured surfaces ranges from 0.20 to 0.22, but the value for textured samples varies from 0.072 to 0.10, demonstrating that boundary and mixed lubrication define the lubrication regime. The untextured surfaces show a higher value of the coefficient of friction compared to the textured one. The coefficient of friction shows a decrease in the value with a slight increase at 2 m/s. The lubricant added to the sliding surface form a boundary lubricated film during the revolutions. Figures 5.23 (a and b) show parallel scratches in the sliding direction depicting the abrasive wear of the surface caused by the worn particles. The lubrication becomes more efficient, and the wear rate reduces, with increasing speed, as shown in Fig. 5.12. However, the lubricant film becomes thinner and exhausts with the number of cycles in the limited supply, which is evident at 1.4 m/s and 2 m/s. As the sliding speed increases, the surfaces indicate a plastically deformed layer appearing, probably due to frictional heating under 30 N load and signs of mild adhesive wear. As illustrated in Fig. 5.5, this also aids in friction reduction.

The morphology of CT7 shows worn-out bulges around the brim and the presence of minor scratches along the wear track. The scratches could be created by worn particles trapped beneath the contact. Figure 5.38 illustrates the average coefficient of friction of 0.084 at 0.2 m/s, which increases to 0.096 at 1.4 m/s before showing a decrease to 0.089 with an increase in the speed to 2 m/s. This indicates the coefficient of friction lower than 0.10 suggesting a

mixed regime of lubrication for CT7. However, a fluctuating trend in coefficient of friction is observed at lower speeds of 0.2 m/s, 0.8 m/s and 1.4 m/s probably due to instable lubricant film (Fig. 5.2 b). At 2 m/s, the CT7 is shown to have best performance under 30 N load. The SEM images of CT20, BT7, and BT20 show morphologies similar to CT7, as observed in Figs. 5.25, 5.26 and 5.27. The wearing out of marginal turn-up after few runs and the presence of worn particles, thereby under the contact, generate grooves along the wear track. The coefficient of friction of CT20 is varying 0.091 to 0.097 compared to BT20, which ranges from 0.072 at lower speed to 0.098 at 2 m/s. The coefficient of friction fluctuates for all cycles at a lower speed of 0.2 m/s, highlighting the possibility of an unstable lubrication film and stick-slip behaviour (Figs 5.2 c-e). Figure 5.5 depicts a higher average coefficient of friction at 0.2 m/s and 1.4 m/s for 7% and 20% densities of circular dimples. This is probably because of less effectiveness of dimple density of CT7 and CT20 for pressure build-up. Both the texture shapes with 7% and 20% densities show mixed lubrication regimes at 30 N load for all the speeds, with some instability of the lubricant film at lower speeds. Because of the reduced contact between the surfaces and the lower coefficient of friction, the surfaces show relatively minor initial wear. Under these working conditions, a lower density of dimples, notably BT7, demonstrates greater performance.

In the study under 50 N load, the textured surfaces exhibit a different behaviour than those shown at 10 N and 30 N loads (Fig. 5.14-13). The friction and wear behaviour of the untextured specimen can be explained by worn surface morphology given in Fig. 5.28 (a-d). As illustrated in Fig. 5.6, the untextured surface has a greater average coefficient of friction than the textured one. In the presence of the lubricant, the boundary lubrication regime is present (Fig. 5.39). As the sliding speed increases, more efficient lubrication is accomplished, resulting in a modest drop in the coefficient of friction from 0.20 to 0.17. Furthermore, the presence of lubricant in the contact zone reduces friction heat. However, because of the limited

supply, the lubricant exhausts after a few passes, causing frictional heating on the surface due to high load of 50 N and speed. As seen in Fig. 5.28, this results in the creation of a compacted layer of worn particles across the surface, minimising friction and wear while avoiding direct metal-to-metal contact. The wear rate also decreases as the speed increases, which is higher than in the textured specimens (Fig. 5.13).

CT7, BT7 and CT20 show a reduction in the average coefficient of friction with increasing speed. BT20 shows an increase in the value from 0.11 to 0.17 with increasing speed. The wear rate of textured specimens shows an initial decrease which increase later at higher speeds. The behaviour can be explained based on the worn surface morphologies. CT7 exhibits a boundary lubrication mechanism under 50 N load at all speeds, as shown in Figs. 5.39 (a-d). A direct surface contact might have occurred, leading to wear of the surface. Grooves can be seen running the length of the track, which are most likely created by worn particles trapped under the sliding surface (Fig. 5.39 a). Wear particles filled in the dimples and present along the wear track at 0.8 m/s may be seen on the surface (Fig. 5.39 b). Frictional heating has also caused a compacted layer of particles to accumulate on the surface. At higher speeds of 1.4 and 2 m/s, the dimple seems to fill, and a layer of compacted particles can be seen along the wear track, as illustrated in Fig. 5.29 (c) and (d). This benefits in the decrease of wear and coefficient of friction. The variation in the coefficient of friction exhibited in Fig. 5.3 (b) at different speeds, on the other hand, can be explained by the aforementioned tribo-pairs contact. At lower speed of 0.2 m/s and 0.8 m/s, BT7 remains in boundary lubrication, and a direct contact between the surfaces cause stick-slip behaviour leading to fluctuation of coefficient of friction (Fig. 5.3 d). As illustrated in Figs. 5.39 (c and d), BT7 remains in the mixed lubrication regime at 1.4 m/s and 2 m/s. The formation of the transfer layer is also observed in worn surface morphology of BT7 shown in Figs. 5.31 (c and d), this indicates the reduction in coefficient of friction is the synergetic effect of lubrication and the oxide layer. The similar behaviour is

observed for CT20 at 2 m/s and under 50 N load. BT20, on the other hand, remains in the boundary lubrication regime at all speeds, resulting in considerable wear on the surface, as illustrated in Fig. 5.32 (a-d). In starved lubrication, the positive effect due to higher density bi-triangular dimples under 50 N load is not apparent. The existence of a greater number of bulged dimples may have resulted in the creation of a greater number of worn particles, resulting in increased wear. This results in a high rate of wear and an increase in the coefficient of friction. This also results in non-uniform friction behaviour, as shown in Fig. 5.3 (e). The positive benefit of surface texturing in starved lubrication is not much beneficial under 50 N load except in a few cases. BT7, however, shows overall better performance, particularly at higher speeds. Circular dimples with 20% density are also shown to have good results at 2 m/s, as obvious from Fig. 5.10.

Fig. 5.40 (a-c) demonstrates the plausible mechanism of friction and wear emphasizing the role of surface textures in dry sliding based on the results of friction and wear and microscopic images of the worn surface along with the wear track. Figure 5.40(a) illustrates the metal-to-metal contact of pin and disc surfaces at the start of the test. As the test proceeds, wear debris is generated due to relative motion at the contact which either gets trapped between the sliding surfaces or fills the dimples or may get ejected from the interface due to centrifugal forces as shown in Fig. 5.40(b). As indicated in Fig. 5.40(c), the dimples are filled with the particles and due to increased friction heating at the interface caused by increasing speed, the trapped debris particles get compacted and form a transfer layer which provides a protective cover to the underlying substrate, reducing friction and wear. The layer breaks after achieving a critical thickness leading to exposure of the metallic surfaces resulting in adhesive wear.

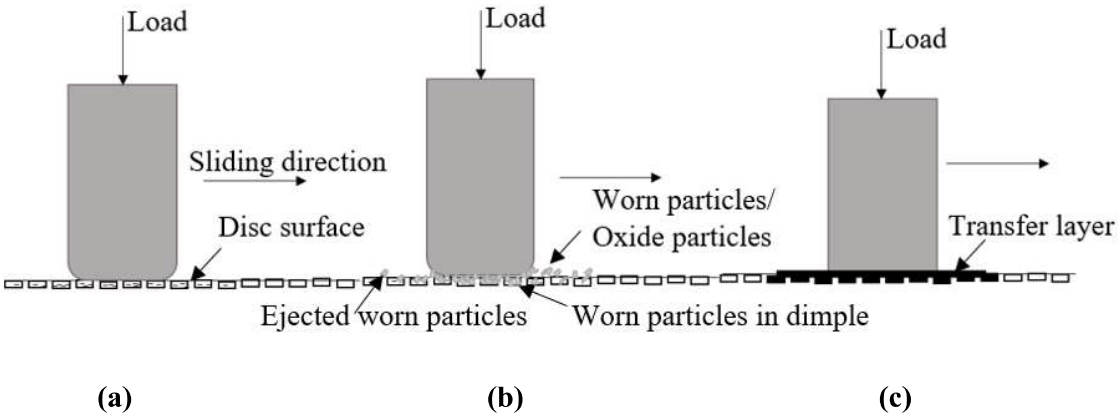

Fig. 5.40 Schematic illustration depicting the plausible friction reduction mechanism under dry sliding condition

Fig. 5.41 (a-c) illustrates the probable mechanism of friction and wear under single-drop lubrication. Initially, the build-up of hydrodynamic pressure results in the separation of two mating bodies as shown in Fig. 5.41(a). Therefore, friction and wear get reduced due to the interposing lubricant between the sliding surfaces. However, because of the limited supply, the lubricant exhausts after several passes, leading to direct metal-to-metal contact and the generation of wear particles that either get accumulated in the dimples or remain on the surface causing an abrasion on the surface as shown in Fig. 5.41(b). However, once the dimples are filled the remaining debris gets compacted in the form of a transfer layer (Fig. 5.41 c) and leads to a reduction in friction as explained earlier. The formation-breakage-reformation of this layer leads to intermittent contact between steel surfaces and leads to adhesive wear and more formation of wear particles. The particles generated through adhesive wear scratch the surface further and result in much wider and deeper grooves.

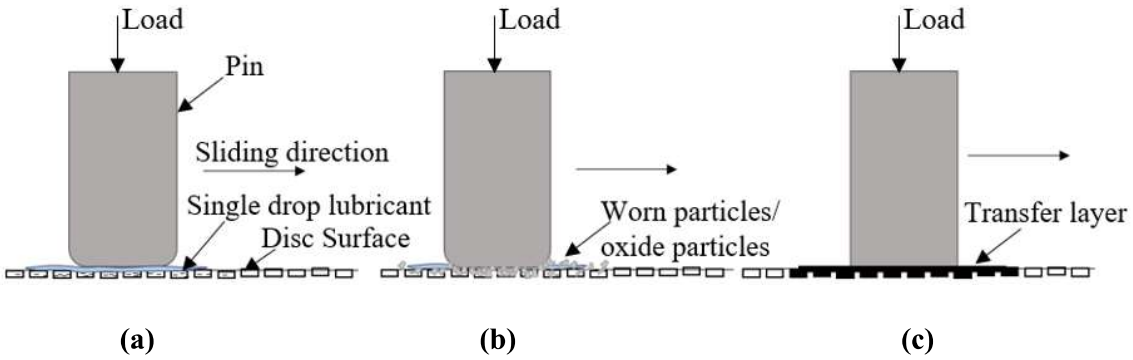

Fig. 5.41 Schematic illustration depicting the probable friction reduction mechanism under single drop lubrication

A comparative assessment of the tribological performance of circular and bi-triangular shapes reveals that the bi-triangular shape with lower density of dimples (7%) is more effective in reducing friction and wear. The result suggests that BT7 having bi-triangular dimples with 7% density, has the optimum performance under the conditions used in the current study. The friction force for a textured surface was reduced by roughly 66% for BT7 when compared to an untextured sample due to surface texturing. Surface texturing with a density of 7% reduced friction force by around 35% compared to the dimple density of 20% for BT7. The texturing of BT7 resulted in about 80% reduction in wear rate. It has been reported that symmetricity of the shape and its alignment in the direction of motion plays an important role in friction reduction. The symmetric shape of the dimple reduces hindrance to the movement of the counter element due to hard deposition if carefully designed, which is not possible in the case of circular or other shapes. Also, longer curved edge helps in better entrapment of loose particles and advancement of lubricants in the cavity. This could be the possible reason for the better performance of the bi-triangular textures in comparison to circular. Surface texturing offers advantages, but it also has drawbacks and depending on the texture qualities, it performs differently under different operating situations. As observed at different speeds from Figs. 7-10, due to the obvious micro-bearing effect, the textured specimens have a load-carrying

capacity and lower average coefficient of friction under 30 N load. If there is no micro-bearing effect, the average coefficient of friction increases as the load increases due to direct surface contact and the presence of worn particles on the contact surface.

When evaluated under a 10 N load, the durability of CT20 is limited to 8000 to 14000 cycles for different speeds, as illustrated in Fig. 5.36. Surface textures can, however, be mixed with solid lubricant coatings to boost longevity in such instances, as previously mentioned. (Jianliang Li et al., 2010). On the basis of the results and discussion above it may be concluded that there is a lifetime for the textures during which they effectively serve their purpose of trapping the wear particles and acting as reservoirs to lubricants under single drop lubrication depending on the conditions of load, speed and probably shape and size of the texture as well.